

Fig. 3. Inflammatory factors upregulated in the lungs of wild-type rats by IT-spraying of TiO<sub>2</sub> particles in the IPS 9 day study (A) SOD activity and (B) 8-OHdG level in wild-type rats treated with TiO<sub>2</sub> particles or saline. (C) MIP1 $\alpha$  protein level was significantly increased (142%) in the lung tissue of wild-type rats treated with TiO<sub>2</sub> (masspam array analysis). MIP1 $\alpha$  was detected in the mammary gland of the TiO<sub>2</sub> group but not in the vehicle group. (D) In western blotting, expression of MIP1 $\alpha$  was increased in the TiO<sub>2</sub> group compared with vehicle group. (E) MIP1 $\alpha$  was immunohistochemically detected in alveolar macrophages containing TiO<sub>2</sub> particles (upper) but was not detected in macrophages of rats that were not exposed to TiO<sub>2</sub> particles (lower).

proliferation of mammary epithelial cells and thereby promoted mammary carcinogenesis. As with the lung, CCR1 was expressed by mammary cells, rendering these cells receptive to MIP1 $\alpha$  induction of proliferation. While MIP1 $\alpha$  secreted by alveolar macrophages would be diluted by the blood volume and while these levels may not be high enough to increase mammary cell proliferation in a short *in vitro* proliferation assay, it is possible that continuous low level stimulation over the course of 12 weeks could increase mammary cell proliferation in the environment of the mammary gland *in vivo*. Another possibility is that TiO<sub>2</sub> particles may act directly on the mammary gland after translocation to the mammary gland from the lung. However, TiO<sub>2</sub> exposure of mammary carcinoma cells did not induce proliferation *in vitro*. It must be understood that promotion of DHPN-induced mammary carcinogenesis by TiO<sub>2</sub> particles was observed in *Hras128* female rats, and these animals are very highly susceptible to mammary carcinogenesis (50). Although, the effects we observed on promotion of mammary carcinogenesis in these animals may not be directly relevant to most humans, people at high risk for mammary

carcinogenesis, such as individuals harboring BRCA mutations, may be a relevant population as regards the risk presented by nanoscale TiO<sub>2</sub>.

Although our observations are based on results obtained with a mixed population of nanoscale and larger sized particle aggregates, size analysis indicated that 80.1% of them were nanoscale (<100 nm in diameter) in the 16 week IPS-initiation-promotion study and 76.6% were nanoscale in the IPS 9 day study. Thus, the results can be interpreted as being strongly associated with nanoscale particle aggregates.

In conclusion, the IPS-initiation-promotion protocol detected TiO<sub>2</sub> carcinogenic activity in the rat lung and is therefore comparable, at least for TiO<sub>2</sub> inhalation, to a long-term whole body inhalation carcinogenesis study. We also elucidated a plausible mechanism for the carcinogenic effect of TiO<sub>2</sub> particles in the rat lung. Phagocytosis of TiO<sub>2</sub> particles by alveolar macrophages resulted in ROS production and DNA damage and increased expression of MIP1 $\alpha$ . MIP1 $\alpha$  in turn was able to enhance proliferation of lung epithelium cells. Thus, lung

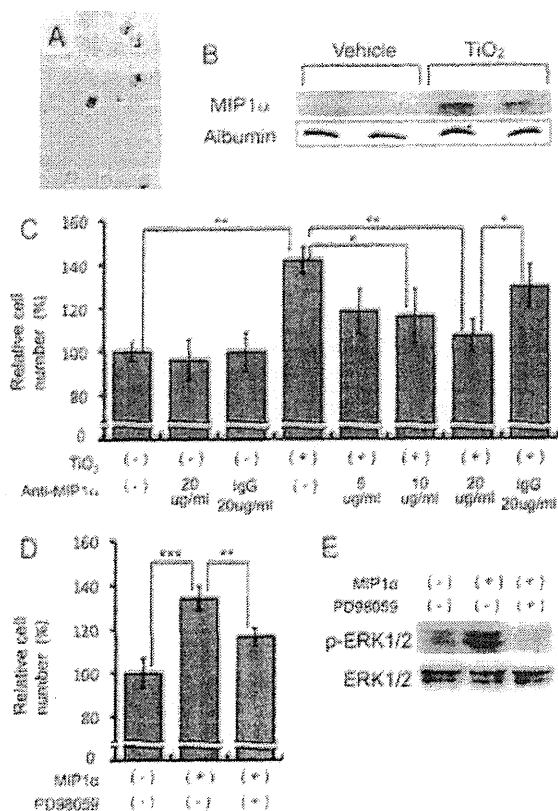


**Fig. 4.** Growth stimulation effects of conditioned medium from alveolar macrophages on human lung cancer cell lines. (A) Primary cultured alveolar macrophages of rats were treated with TiO<sub>2</sub> particles. (B) MIP1 $\alpha$  was detected in the culture medium. (C) The number of A549 cells was significantly increased by addition of conditioned medium from alveolar macrophages treated with TiO<sub>2</sub> particles. MIP1 $\alpha$  neutralizing antibody attenuated this effect in a dose-dependent manner. Irrelevant IgG was used as control antibody. (D) MIP1 $\alpha$ -induced cell proliferation was significantly suppressed by the ERK inhibitor PD98059. (E) MIP1 $\alpha$  increased ERK phosphorylation and PD98059 diminished this phosphorylation.

tissue exposed to TiO<sub>2</sub> particles exhibits increase in both DNA damage and proliferation. Importantly, a similar mechanism would function in humans in the promotion of lung carcinogenesis associated with inhalation of TiO<sub>2</sub> particles and other nanoparticles with the capacity to form aggregates. In addition, TiO<sub>2</sub> administered to the lung had carcinogenic activity in the *Hras*128 transgenic rat mammary gland; this carcinogenic activity is probably mediated via serum MIP1 $\alpha$  resulting from expression of MIP1 $\alpha$  by alveolar macrophages. This finding may indicate that exposure of TiO<sub>2</sub> particles is a risk factor for mammary carcinogenesis in predisposed populations, such as individuals with BRCA mutations.

**Supplementary material**

Supplementary Figures 1–3 and Tables 1 and 2 can be found at <http://carcin.oxfordjournals.org/>

**Funding**

Health and Labour Sciences Research Grants, Ministry of Health, Labour and Welfare, Japan (Research on Risk of Chemical Substance 21340601, H18-kagaku-ippan-007); a grant-in-aid for the Second

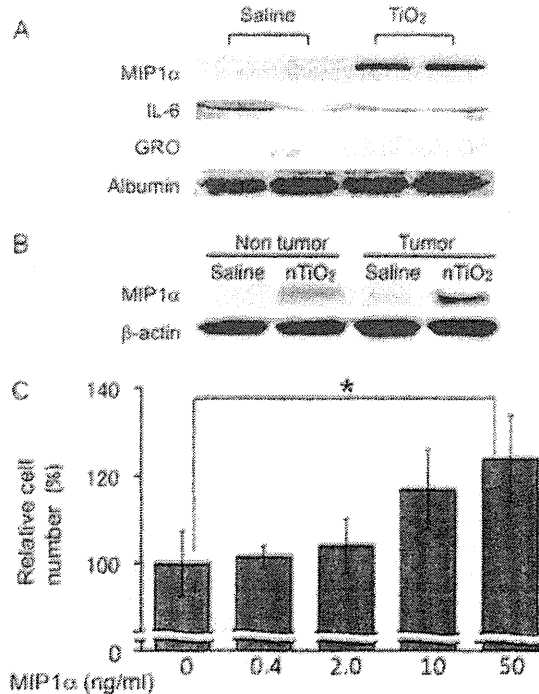


**Fig. 5.** Promotion effects of MIP1 $\alpha$  on proliferation of a rat mammary cancer cell line, C3 (A) MIP1 $\alpha$  was detected in the serum of the *Hras*128 rats treated with TiO<sub>2</sub> but not in vehicle control rats in the 16 week study. No difference in IL-6 in the serum was observed and GRO was not detected in the serum. (B) MIP1 $\alpha$  levels are slightly elevated in non-tumor and tumor tissue of the mammary gland of animals treated by IPS with TiO<sub>2</sub> particles in the 16 week study. (C) Recombinant MIP1 $\alpha$  increased the number of rat mammary carcinoma C3 cells in a dose-dependent manner ( $P = 0.0127$ ).

Term Comprehensive 10 Year Strategy for Cancer Control, Ministry of Health, Labour and Welfare, Japan; grants-aid for Cancer Research, Ministry of Education, Culture, Sports, Science and Technology.

**Acknowledgements**

*Conflict of Interest Statement:* None declared.

**References**

- Obendorfster, G. (2002) Toxicokinetics and effects of fibrous and nonfibrous particles. *Inhal. Toxicol.*, **14**, 29–56.
- Ramundstad, P. et al. (2001) Cancer incidence among workers in the Norwegian silicon carbide industry. *Am. J. Epidemiol.*, **153**, 978–986.
- Pott, F. et al. (2005) Carcinogenicity study with nineteen granular dusts in rats. *Eur. J. Oncol.*, **10**, 249–281.
- Baan, R. et al. (2006) Carcinogenicity of carbon black, titanium dioxide, and talc. *Lancet Oncol.*, **7**, 295–296.
- Schulte, P. et al. (2008) Occupational risk management of engineered nanoparticles. *J. Occup. Environ. Hyg.*, **5**, 239–249.
- Maynard, A.D. et al. (2006) Safe handling of nanotechnology. *Nature*, **444**, 267–269.
- Scharinger, M. (2008) Nanotoxicology: environmental risks of nanomaterials. *Nat. Nanotechnol.*, **3**, 322–323.
- Born, P. et al. (2006) Research strategies for safety evaluation of nanomaterials, part V: role of dissolution in biological fate and effects of nanoscale particles. *Toxicol. Sci.*, **90**, 23–33.
- Pfaffen, R.F. (1976) Inhalation exposure of animals. *Environ. Health Perspect.*, **16**, 17–24.

10. Mauderly, J.L. (1997) Relevance of particle-induced rat lung tumors for assessing lung carcinogenic hazard and human lung cancer risk. *Environ. Health Perspect.*, **105** (suppl. 5), 1337-1346.
11. Roller, M. *et al.* (2006) Lung tumor risk estimates from rat studies with non-specifically toxic granular dusts. *Ann. N. Y. Acad. Sci.*, **1076**, 266-280.
12. Imada, K. *et al.* (1996) Initiation-promotion model for assessment of carcinogenicity: medium-term liver bioassay in rats for rapid detection of carcinogenic agents. *J. Toxicol. Sci.*, **21**, 483-487.
13. IARC (1999) The use of short- and medium-term tests for carcinogens and data on genetic effects in carcinogenic hazard evaluation. Consensus report. *IARC Sci. Publ.*, **146**, 1-18.
14. Asamoto, M. *et al.* (2000) Transgenic rats carrying human c-Ha-ras proto-oncogenes are highly susceptible to N-methyl-N-nitrosourea mammary carcinogenesis. *Carcinogenesis*, **21**, 243-249.
15. Han, B.S. *et al.* (2002) Inhibitory effects of 17 $\beta$ -estradiol and 4-n-octylphenol on 7,12-dimethylbenz[*a*]anthracene-induced mammary tumor development in human c-Ha-ras proto-oncogene transgenic rats. *Carcinogenesis*, **23**, 1209-1215.
16. Ohnishi, T. *et al.* (2007) Possible application of human c-Ha-ras proto-oncogene transgenic rats in a medium-term bioassay model for carcinogens. *Toxicol. Pathol.*, **35**, 436-443.
17. Torres, E. *et al.* (2005) Significance of macrophage inflammatory protein-1 alpha (MIP-1alpha) in multiple myeloma. *Leuk. Lymphoma*, **46**, 1699-1707.
18. Driscoll, K.E. *et al.* (1993) Macrophage inflammatory proteins 1 and 2: expression by rat alveolar macrophages, fibroblasts, and epithelial cells and in rat lung after mineral dust exposure. *Am. J. Respir. Cell Mol. Biol.*, **8**, 311-318.
19. Hamaguchi, T. *et al.* (2006) Establishment of an apoptosis-sensitive ras mammary carcinoma cell line with a mutation in the DNA-binding region of p53. *Cancer Lett.*, **232**, 279-288.
20. IARC (1989) Titanium dioxide. *IARC monograph Evaluation of carcinogenic risks to humans*. IARC Scientific Publications, Lyon, vol. 47, pp. 307-326.
21. Stoner, G.D. *et al.* (1993) Lung tumors in strain A mice: application for studies in cancer chemoprevention. *J. Cell. Biochem. Suppl.*, **17E**, 95-103.
22. Pinc, H.C. *et al.* (1978) Biochemical characterization of stages of hepatocarcinogenesis after a single dose of diethylnitrosamine. *Nature*, **271**, 456-458.
23. Peraino, C. *et al.* (1971) Reduction and enhancement by phenobarbital of hepatocarcinogenesis induced in the rat by 2-acetylaminofluorene. *Cancer Res.*, **31**, 1506-1512.
24. Ito, N. *et al.* (2003) A medium-term rat liver bioassay for rapid *in vivo* detection of carcinogenic potential of chemicals. *Cancer Sci.*, **94**, 3-8.
25. Ito, N. *et al.* (1988) Wide-spectrum initiation models: possible applications to medium-term multiple organ bioassays for carcinogenesis modifiers. *Jpn. J. Cancer Res.*, **79**, 413-417.
26. IARC (1980) Long-term and short-term screening assays for carcinogens: a critical appraisal. *IARC Scientific Publications*, Lyon, vol. 83 (suppl. 2), pp. 1-146.
27. Konishi, Y. *et al.* (1987) Lung carcinogenesis by N-nitrosobis(2-hydroxypropyl)amine-related compounds and their formation in rats. *IARC Sci. Publ.*, **82**, 250-252.
28. Nishikawa, A. *et al.* (1994) Effects of cigarette smoke on N-nitrosobis(2-oxopropyl)amine-induced pancreatic and respiratory tumorigenesis in hamsters. *Jpn. J. Cancer Res.*, **85**, 1000-1004.
29. Yamazaki, K. *et al.* (1996) Exposure to dimethylarsinic acid, a main metabolite of inorganic arsenic, strongly promotes tumorigenesis initiated by 4-nitroquinoline 1-oxide in the lungs of mice. *Carcinogenesis*, **17**, 767-770.
30. Rom, W.N. *et al.* (1991) Cellular and molecular basis of the asbestos-related diseases. *Am. Rev. Respir. Dis.*, **143**, 408-422.
31. Heppleston, A.G. (1984) Pulmonary toxicology of silica, coal and asbestos. *Environ. Health Perspect.*, **55**, 111-127.
32. Renwick, L.C. *et al.* (2001) Impairment of alveolar macrophage phagocytosis by ultraline particles. *Toxicol. Appl. Pharmacol.*, **172**, 119-127.
33. Rimal, B. *et al.* (2005) Basic pathogenetic mechanisms in silicosis: current understanding. *Curr. Opin. Pulm. Med.*, **11**, 169-173.
34. Wang, Y. *et al.* (2007) The role of the NADPH oxidase complex, p38 MAPK, and Akt in regulating human monocyte/macrophage survival. *Am. J. Respir. Cell Mol. Biol.*, **36**, 68-77.
35. Bhatt, N.Y. *et al.* (2002) Macrophage colony-stimulating factor-induced activation of extracellular-regulated kinase involves phosphatidylinositol 3-kinase and reactive oxygen species in human monocytes. *J. Immunol.*, **169**, 6427-6434.
36. Dorger, M. *et al.* (2000) Comparison of the phagocytic response of rat and hamster alveolar macrophages to man-made vitreous fibers *in vitro*. *Hum. Exp. Toxicol.*, **19**, 635-640.
37. Blake, T. *et al.* (1998) Effect of fiber length on glass microfiber cytotoxicity. *J. Toxicol. Environ. Health A*, **54**, 243-259.
38. Kibir, S. *et al.* (1995) Serum levels of interleukin-1, interleukin-6 and tumour necrosis factor-alpha in patients with gastric carcinoma. *Cancer Lett.*, **95**, 207-212.
39. Schneider, M.R. *et al.* (2000) Interleukin-6 stimulates clonogenic growth of primary and metastatic human colon carcinoma cells. *Cancer Lett.*, **151**, 31-38.
40. Asselin-Paturel, C. *et al.* (1998) Quantitative analysis of Th1, Th2 and TGF- $\beta$ 1 cytokine expression in tumor, TH, and PBL of non-small cell lung cancer patients. *Int. J. Cancer*, **77**, 7-12.
41. Matanic, D. *et al.* (2003) Cytokines in patients with lung cancer. *Scand. J. Immunol.*, **57**, 173-178.
42. Brichary, F.M. *et al.* (2001) An immune response manifested by the common occurrence of annexins I and II autoantibodies and high circulating levels of IL-6 in lung cancer. *Proc. Natl Acad. Sci. USA*, **98**, 9824-9829.
43. Rollins, B.J. (1997) Chemokines. *Blood*, **90**, 909-928.
44. Zhou, Y. *et al.* (2005) The chemokine GRO-alpha (CXCL1) confers increased tumorigenicity to glioma cells. *Carcinogenesis*, **26**, 2058-2068.
45. Yang, G. *et al.* (2006) The chemokine growth-regulated oncogene 1 (Gro-1) links RAS signaling to the senescence of stromal fibroblasts and ovarian tumorigenesis. *Proc. Natl Acad. Sci. USA*, **103**, 16472-16477.
46. Li, A. *et al.* (2004) Constitutive expression of growth regulated oncogene (gro) in human colon carcinoma cells with different metastatic potential and its role in regulating their metastatic phenotype. *Clin. Exp. Metastasis*, **21**, 571-579.
47. Rollins, B.J. (2006) Inflammatory chemokines in cancer growth and progression. *Eur. J. Cancer*, **42**, 760-767.
48. Lentzsch, S. *et al.* (2003) Macrophage inflammatory protein 1-alpha (MIP-1 alpha) triggers migration and signaling cascades mediating survival and proliferation in multiple myeloma (MM) cells. *Blood*, **101**, 3568-3573.
49. Baggs, R.B. *et al.* (1997) Regression of pulmonary lesions produced by inhaled titanium dioxide in rats. *Vet. Pathol.*, **34**, 592-597.
50. Tsuchi, H. *et al.* (2001) High susceptibility of transgenic rats carrying the human c-Ha-ras proto-oncogene to chemically-induced mammary carcinogenesis. *Mutat. Res.*, **477**, 173-182.

Received September 27, 2009; revised January 14, 2010;  
accepted January 24, 2010

## SYMPOSIUM PRESENTATION

## Risk Assessment Studies of Nanomaterials in Japan and Other Countries

Hiroyuki Tsuda

## Abstract

Recent developments in nanoparticle (NP) technology and their commercial production have raised concern regarding NP risk to health and the environment. The toxicological characteristics of NP may not be similar to that observed in pre-NP materials because of the enormous differences in size and surface area. Thus, careful risk evaluation studies are required. Since some NP have already been produced and introduced into the market, before a suitable framework enabling risk management has been firmly established, toxicological studies based on the specificity of NP which are not subordinate to their commercial production are indispensable. The summary of nanotoxicology studies shown below clearly indicates that compared with the UK, EU, USA, and other countries, Japanese studies regarding metals and SWCNT are far from sufficient to evaluate risk.

**Key Words:** Nanoparticles - toxicology - carcinogenicity - titanium dioxide - carbon black




*Asian Pacific J Cancer Prev*, 10, DIMS Supplement 11-12

## Introduction

The safety of our living environment can be secured by the balanced function of three elements: risk assessment, risk management and risk communication. The first of these elements, risk assessment, must be addressed first, since without reliable risk assessment, risk communication and risk management can not function. Importantly, for reliable risk assessment long-term animal studies are indispensable.

These principles, of course, hold true for engineered nanoparticles. Unfortunately, the risk assessment data for engineered nanoparticles are rather fragmentary. However, the available findings do present a disturbing picture of potential carcinogens entering the market place. Engineered nanoparticles included in this review include nano-size titanium dioxide (nTiO<sub>2</sub>), carbon black (nCB), single-walled carbon nanotubes (SWCNT), multiple-walled carbon nanotubes (MWCNT) and fullerenes

**Table 1. Number of Subacute/Chronic Toxicity Tests (PubMed, ~2007)**

				Total
TiO <sub>2</sub>	1	2	2 <sup>a</sup>	<del>5</del> 5
S MW-CNT	2			<del>2</del> 2
Fullerenes		1		1
UF-Carbon black			4 <sup>a</sup>	4
Total	0	3	6	9

<sup>a</sup>Carcinogenic

*Nanotoxicology Project, Department of Molecular Toxicology, Nagoya City University Graduate School of Medical Sciences  
1 Kawasumi, Mizuho-cho, Mizuho-ku, Nagoya 467-8601, Japan*

(C60). A summary of the testing so far performed shows that data are limited and Japan is not putting the priority this subject deserves (see Table 1) and Tsuda et al (2009), for a review.

## Overall Evaluation and Proposal for the Future

During the development and marketing of nanomaterials, risk assessment of these new products has been perfunctory at best. While nanomaterials have undeniable benefits, their use also has undeniable potential risk. This risk must be addressed in an unbiased and thorough manner. Only after the toxicity of the various nanomaterials is understood can their true benefits be realized.

In rodent studies, nTiO<sub>2</sub> whether administered by inhalation or intratracheal instillation was shown to induce lung tumors with characteristic squamous cell morphology in female rats. These nanomaterials did not induce lung tumors in male rats. Our own studies have also shown that instillation of nTiO<sub>2</sub> into the lungs of female rats showed tumor promoting activity and resulted in elevated ROS-mediated damage and production of inflammatory cytokines. It is reasonable to assume that other metal-derived nanoparticles, such as aluminium and copper nanoparticles, and metal containing nanoparticles, for example nCB-metal mixtures and SWCNT and MWCNT preparations, are also capable of producing these effects.

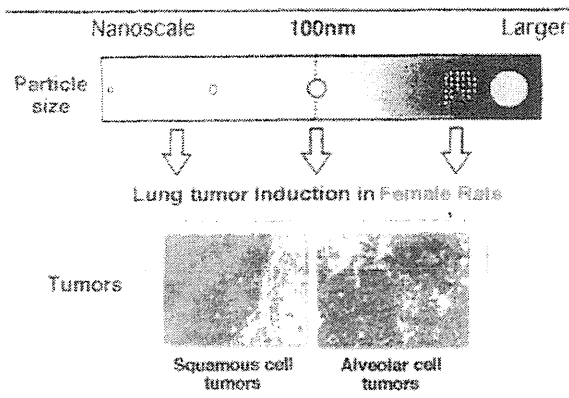


**Figure 1. Schematic Presentation of Carcinogenic Effects of  $\text{TiO}_2$ , Carbon Black.** Carcinogenic effects were elicited by both nano-scale and larger sized particles

Nanoparticles such as  $\text{nTiO}_2$ ,  $\text{nCB}$ , SWCNT and MWCNT when intratracheally administered, were detected by light microscope as aggregates or agglomerates and these forms are reported to induce foreign body granulation tissue with various degree of inflammatory reaction. Although the relevance of foreign body-induced chronic inflammation to carcinogenesis is not clearly established, it is possible that reactive oxygen species (ROS) produced by macrophages attempting to destroy the foreign material in the inflammation site may cause DNA damage associated with carcinogenesis. Another possible contributing factor is metal, for example from metal-derived nanoparticles such as  $\text{TiO}_2$  or from metal contaminants: these metals could also be involved in ROS production. Thus, it is possible that the observed carcinogenic effect is not specific to nanoparticles but rather associated with their ability to induce persistent foreign body-induced chronic inflammation and/or introduce metals into susceptible sites. For example,  $\text{TiO}_2$  and carbon blacks larger than 100nm in diameter are known to induce lung tumors including similar squamous cell morphology (Nikula, 2000); (Pott and Roller, 2005) and both of these materials (larger than nano size) are classified as into group 2B (possibly carcinogenic to humans) by WHO/IARC (see Figure 1).

Mechanisms for mesothelioma induction by MWCNT in mice and rats have not been elucidated yet. A possible contributing factor is metal: Transition metals, such as iron, are commonly used as a catalytic center in the formation of CNTs, and contaminating metal in SWCNT and MWCNT particles could catalyze the formation of ROS by the Fenton reaction (Liu and Okada, 1994). One example of this type of toxicity is that human keratinocytes exposed to SWCNT were killed by ROS in the media (Shvedova et al., 2003). Another possible contributing factor is the length of the MWCNT (Pott and Roller, 2005; Muller et al., 2009; Sakamoto et al., 2009).

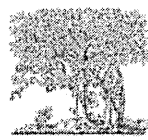
As noted at the beginning of this review, for reliable risk assessment long-term animal studies are indispensable. This is particularly true for risk assessment of potential carcinogens. The standard for the evaluation of the carcinogenic potential of a test chemical is testing

in two rodent species, generally rats and mice, of each sex, at 3 doses (0, low and high) of the test chemical for up to two years. In the studies conducted to date concerning the carcinogenic risk presented by nanoparticles, there is a noticeable lack of long term testing: No long-term tests of any type have been reported for either SWCNT or fullerenes. Importantly, the primary goal of risk assessment is not to simply ban a product from the market place, but rather to determine product safety and establish guidelines lines for its production and use and promote consumer confidence. Given the known ability of many nanomaterials to induce mechanisms which are active in humans that are risk factors for carcinogenesis, for example ROS and inflammatory cytokine production, the continued introduction of these materials into the market is alarming. Establishing the safety of these materials is urgently needed.

In this short review, available in vivo data concerning the carcinogenic effects of  $\text{nTiO}_2$ ,  $\text{nCB}$ , SWCNT and MWCNT, and Fullerenes is outlined. Of these,  $\text{nTiO}_2$  and  $\text{nCB}$  are classified as possibly carcinogenic to humans. Testing of the carcinogenic activity of MWCNT produced mixed results. SWCNT and fullerenes have no carcinogenic activity in the studies conducted to date, however, toxicity testing of these materials has been quite limited and both of these materials have the potential to produce ROS. The observations noted here may apply to possible carcinogenic risk of other nanoparticles because of shared mechanisms of induction of inflammatory lesions and ROS generation. Our conclusions are that nanoparticles are clearly potentially toxic/carcinogenic to humans and their toxicity must be assessed, and their production and use managed appropriately.

## References

- Liu M, Okada S (1994). Induction of free radicals and tumors in the kidneys of Wistar rats by ferric ethylenediamine- $\text{N,N}'$ -diacetate. *Carcinogenesis*, **15**, 2817-21.
- Muller J, Delos M, Panin N, et al (2009). Absence of carcinogenic response to multiwall carbon nanotubes in a 2-year bioassay in the peritoneal cavity of the rat. *Toxicol Sci*, **110**, 442-8.
- Muller J, Huaux F, Moreau N, et al (2005). Respiratory toxicity of multi-wall carbon nanotubes. *Toxicol Appl Pharmacol*, **207**, 221-31.
- Nikula KJ (2000). Rat lung tumors induced by exposure to selected poorly soluble nonfibrous particles. *Inhal Toxicol*, **12**, 97-119.
- Pott F, Roller M (2005). Carcinogenicity study with nineteen granular dusts in rats. *Eur J Oncol*, **10**, 249.
- Sakamoto Y, Nakae D, Fukumori N, et al (2009). Induction of mesothelioma by a single intrascrotal administration of multi-wall carbon nanotube in intact male Fischer 344 rats. *J Toxicol Sci*, **34**, 65-76.
- Shvedova AA, Castranova V, Kisin ER, et al (2003). Exposure to carbon nanotube material: assessment of nanotube cytotoxicity using human keratinocyte cells. *J Toxicol Environ Health A*, **66**, 1909-26.
- Tsuda H, Xu J, Sakai Y, Futakuchi M, Fukamachi K (2009). Toxicology of engineered nanomaterials - A review of carcinogenic potential. *Asian Pacific J Cancer Prev*, **10**, 975-80.



ELSEVIER

Contents lists available at ScienceDirect

## Food and Chemical Toxicology

journal homepage: [www.elsevier.com/locate/foodchemtox](http://www.elsevier.com/locate/foodchemtox)

## Lack of promoting effect of titanium dioxide particles on ultraviolet B-initiated skin carcinogenesis in rats

Jiegou Xu<sup>a,c</sup>, Yoko Sagawa<sup>b</sup>, Mitsuru Futakuchi<sup>a</sup>, Katsumi Fukamachi<sup>a</sup>, David B. Alexander<sup>a,c</sup>, Fumio Furukawa<sup>c</sup>, Yoshiaki Ikarashi<sup>d</sup>, Tadashi Uchino<sup>d</sup>, Tetsuji Nishimura<sup>d</sup>, Akimichi Morita<sup>b</sup>, Masumi Suzui<sup>a</sup>, Hiroyuki Tsuda<sup>e,\*</sup><sup>a</sup> Department of Molecular Toxicology, Nagoya City University Graduate School of Medical Sciences, 1-Kawasumi, Mizuho-cho, Minho-ku, Nagoya 467-8601, Japan<sup>b</sup> Department of Dermatology, Nagoya City University Graduate School of Medical Sciences, 1-Kawasumi, Mizuho-cho, Mizuho-ku, Nagoya 467-8601, Japan<sup>c</sup> Daiyukai Institute of Medical Science, Inc., 64 Coura, Nishi-zaai, Azai-cho, Ichinomiya 491-0113, Japan<sup>d</sup> National Institute of Health Sciences, 1-18-1 Kamiyoga, Setagaya-ku, Tokyo 158-8501, Japan<sup>e</sup> Laboratory of Nanotoxicology Project, Nagoya City University, 3-1 Tanobedohri, Mizuho-ku, Nagoya 467-8603, Japan

## ARTICLE INFO

## Article history:

Received 15 October 2010

Accepted 9 March 2011

Available online 15 March 2011

## Keywords:

TiO<sub>2</sub>

Nano-size

Skin

Mammary gland

Carcinogenesis

UVB

## ABSTRACT

Titanium dioxide (TiO<sub>2</sub>) is used in sunscreens and cosmetics as an ultraviolet light screen. TiO<sub>2</sub> has carcinogenic activity in the rat lung, but its effect on the skin has not been reported. We examined the promoting/carcinogenic effect of nano-size TiO<sub>2</sub> particles using a two-stage skin model. c-Ha-ras proto-oncogene transgenic (Hras128) rats, which are sensitive to skin carcinogenesis, and their wild-type siblings were exposed to ultraviolet B radiation on shaved back skin twice weekly for 10 weeks; then the shaved area was painted with a 100 mg/ml TiO<sub>2</sub> suspension twice weekly until sacrifice. All rats were killed at week 52 except for female Hras128 rats which were sacrificed at week 16 because of early mammary tumor development. Skin tumors developed in male Hras128 rats and mammary tumors developed in both sexes of Hras128 rats and in wild-type female rats, but tumor incidence was not different from controls. TiO<sub>2</sub> particles were detected in the upper stratum corneum but not in the underlying skin tissue layers. TiO<sub>2</sub> particles also did not penetrate a human epidermis model *in vitro*. Our data suggest that TiO<sub>2</sub> does not cause skin carcinogenesis, probably due to its inability to penetrate through the epidermis and reach underlying skin structures.

© 2011 Elsevier Ltd. All rights reserved.

## 1. Introduction

Titanium dioxide (TiO<sub>2</sub>) is a wide spectrum physical sunscreen (Anderson et al., 1997) and is used in sunscreen formulations to protect against UV radiation-related skin lesions (Celis et al., 2003; Rouabhia et al., 2002; Suzuki, 1987). TiO<sub>2</sub> nanoparticles have been introduced into sunscreen and cosmetics formulations recently to improve their physical properties, e.g., make them more transparent and less viscous, without losing their UV light blocking ability (Newman et al., 2009). Nanoparticles, defined as having at least one dimension of 100 nm or less (ISO, 2008), were postulated to be able to penetrate the stratum corneum and diffuse into underlying skin structures, which gives rise to concerns about potential health risks (Newman et al., 2009; Nohynek et al., 2008). In

human skin samples, topically applied tetramethylammonium hydroxide nanoparticles and sodium bis(2-ethylhexyl) sulfosuccinate nanoparticles get into the hair follicles and the stratum corneum and reach the viable epidermis (Baroli et al., 2007). Dermal administered near-infrared quantum dot nanoparticles can localize, possibly via skin macrophages and Langerhans cells, to regional lymph nodes (Kim et al., 2004). These findings and the report that endothelial cells have the capacity to internalize nanoparticles (Peters et al., 2004) suggests the possibility of potential pro-inflammatory, cytotoxic or other harmful effects.

TiO<sub>2</sub> particles including micro- and nano-sized, are evaluated as a Group 2B carcinogen by WHO/International Agency for Research on Cancer (IARC) (Baan et al., 2006), based on 2-year animal aerosol inhalation studies (Lee et al., 1985; Pott and Roemer, 2005). The mechanism of lung carcinogenesis involves MIP1α derived from TiO<sub>2</sub>-laden alveolar macrophages (Xu et al., 2010). Therefore, it is possible that TiO<sub>2</sub> particles may be carcinogenic to the skin and subcutaneous tissues if they penetrate into the epidermis and cause inflammatory lesions, including enhanced macrophage

Abbreviations: TiO<sub>2</sub>, titanium dioxide; Hras128 rat, human c-Ha-ras proto-oncogene transgenic rat; UVB, ultraviolet B light.

\* Corresponding author. Tel.: +81 52 836 3496; fax: +81 52 836 3497.

E-mail address: [htsuda@med.nagoya-cu.ac.jp](mailto:htsuda@med.nagoya-cu.ac.jp) (H. Tsuda).

0278-8915/\$ - see front matter © 2011 Elsevier Ltd. All rights reserved.

doi:10.1016/j.fct.2011.03.011

activity. Consequently, an important issue is whether TiO<sub>2</sub> particles have the ability to penetrate the stratum corneum and reach the epidermis. Pflucker et al. and Mavon et al. reported that when TiO<sub>2</sub> particles, including micro- and nano-sizes, were topically applied repeatedly to human skin samples *in vitro*, only the upper stratum corneum and hair follicles showed any evidence of particle penetration (Mavon et al., 2007; Pflucker et al., 2001). Even in human skin samples after tape stripping, ultrafine TiO<sub>2</sub> did not penetrate beyond the stratum corneum (Gottbrath and Muller-Goymann, 2003). These results suggest that dermal penetration of TiO<sub>2</sub> particles is in fact associated with hair follicle orifice and not due to direct diffusion through the stratum corneum into the epidermis. Contrary to these *in vitro* findings, Wu et al. reported that TiO<sub>2</sub> nanoparticles could penetrate through the stratum corneum and be located in the deep layer of the epidermis after being topically applied to pig ear *in vivo* for 30 days (Wu et al., 2009). This study also reported that TiO<sub>2</sub> nanoparticles reached different tissues and induced diverse pathological lesions in several major organs after 60 days dermal exposure to hairless mice. The difference in skin penetration between *in vitro* and *in vivo* topical application of TiO<sub>2</sub> particles needs further investigation.

Here, we report results of the carcinogenic effect of TiO<sub>2</sub> particles in the skin using a UVB-initiated 2-stage carcinogenesis protocol. For this purpose, human *c-Ha-ras* proto-oncogene transgenic rats (Hras 128) were used because they are more sensitive to chemically induced skin carcinogens than wild-type rats (Park et al., 2004). Our data indicate that TiO<sub>2</sub> did not penetrate through the epidermis and reach the underlying skin structures and did not have skin carcinogenic activity.

## 2. Materials and methods

### 2.1. Animals

Transgenic rats carrying the human *c-Ha-ras* proto-oncogene (Hras128 rats), known to be sensitive to chemically induced skin carcinogenesis in males and mammary carcinogenesis in females, and their wild-type counterparts were maintained and bred by CLEA Japan Co., Ltd. (Tokyo, Japan). The animals were housed in the Animal Center of Nagoya City University Medical School and maintained on a 12 h light/12 h dark cycle and received Oriental MF basal diet (Oriental Yeast Co., Tokyo, Japan) and water *ad libitum*. The study was conducted according to the Guidelines for the Care and Use of Laboratory Animals of Nagoya City University Medical School and the experimental protocol was approved by the Institutional Animal Care and Use Committee (H17-28).

### 2.2. Preparation of titanium dioxide suspension

Ultrafine grade TiO<sub>2</sub> particles (CAS No. 13463-67-7, rutile type, without coating, mean primary diameter of 20 nm, Ishihara Sangyo Kaisha, Ltd., Osaka, Japan) were provided by Japan Cosmetic Association, Tokyo, Japan. TiO<sub>2</sub> particles were suspended at 100 mg/ml in Pentalan 408 (pentastyrthetol tetractylhexamonoate, CAS 7299-99-2, Nipko Chemicals Co., Tokyo, Japan). The suspensions were sonicated for 30 min just before use, since TiO<sub>2</sub> particles are known to form aggregates. The size distribution of the TiO<sub>2</sub> suspension in Pentalan 408 was analyzed by a Particle Size Distribution Analyzer (Shimadzu Techno-Research, Inc., Kyoto, Japan).

### 2.3. Promotion study in the skin

A total of 80 Hras128 rats and their wild-type siblings, of both sexes and aged 10 weeks old, were randomly allocated to three groups after a 1 week acclimation: Group 1 received ultraviolet B (UVB) radiation (UVB radiation unit, Dermaray 100, Eisai-Toshiba, Tokyo, Japan) 2 times per week for 10 weeks at 800 mJ/cm<sup>2</sup>, 7 min, 20 cm distance from the shaved target skin, followed by painting with 0.5 ml of TiO<sub>2</sub> suspended in Pentalan 408 at 100 mg/ml on the shaved area twice a week until sacrifice. Group 2 received UVB radiation and painting with the vehicle Pentalan 408 on the shaved area twice a week until sacrifice, and Group 3 received painting with 0.5 ml of TiO<sub>2</sub> suspension as in Group 1 but without prior UVB radiation. The painting was done gently using a bacterial spreader. The hair of the back was cut in a 3 × 3 cm area with an electric clipper and the remaining hairs were thoroughly shaved with a razor just before every UVB irradiation and/or TiO<sub>2</sub> painting. Any grossly visible papilloma lesions were carefully examined every day (Fig. 1). All the animals were sacrificed at week 52 (after 42 weeks painting) except for the female Hras128 rats which were terminated at week 16 (after 6 weeks painting) due

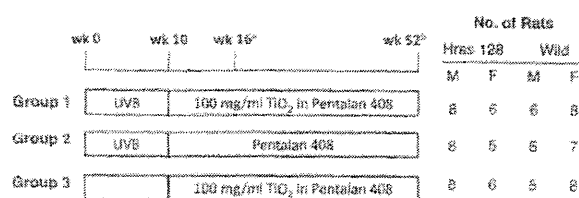


Fig. 1. Schematic of the treatment schedule used to test for skin carcinogenesis in rats. Rats were randomly allocated into three groups: Group 1: UVB radiation for 10 weeks, followed by painting with TiO<sub>2</sub> suspension twice a week; Group 2: UVB radiation for 10 weeks, followed by painting with the vehicle, Pentalan 408, twice a week; and Group 3: painting with TiO<sub>2</sub> suspension twice a week without previous UVB radiation. (a) male Hras128 rats and male and female wild-type rats were sacrificed at week 52 and (b) female Hras128 rats were sacrificed at week 16 due to early mammary tumor development.

to early mammary tumor development. The organs, the skin, brain, lung, liver, mammary gland, mesenteric lymph nodes, spleen and kidney, were excised and fixed in 4% paraformaldehyde solution in PBS buffer adjusted to pH 7.3 and processed for light microscopic examination.

### 2.4. *In vitro* TiO<sub>2</sub> penetration assay

To evaluate whether TiO<sub>2</sub> particles could penetrate into the epidermis, the 12 well LabCyte EPI-MODEL (Japan Tissue Engineering Co., Ltd, Aichi, Japan) was used. Eight wells were exposed to either 43.2 μl of Pentalan 408 alone or 100 or 200 mg/ml of TiO<sub>2</sub> suspended in Pentalan 408 for 48 h. The 24 samples in the receiving chambers were then collected for detection of elemental titanium.

### 2.5. Determination of the elemental titanium

For the detection of elemental titanium, 1 ml of the medium collected from the receiving chambers was treated with 5 ml concentrated HNO<sub>3</sub> for 22 min in a microwave oven. Titanium in the treated solutions was determined by inductively coupled plasma/mass spectrometry (ICP-MS) (HP-4500, Hewlett-Packard Co., Houston, Texas) under the following conditions: RF power-1450 W; RF refraction current-5 W; Plasma gas current-15 L/min; Carrier gas current-0.91 L/min; Perme pump-0.2 rps; Monitoring mass-*m/z* 48 (Ti); Integrating interval-0.1 s; Sampling period 0.31 s.

### 2.6. Cytokine analysis

Five wild-type male Sprague-Dawley rats aged 10 weeks were shaved as described above and painted with 0.5 ml of 100 mg/ml of TiO<sub>2</sub> suspended in Pentalan 408 on the shaved area once a day for 14 consecutive days. Five rats were painted with Pentalan 408 as the control. The painted area was excised, rinsed with cold PBS 3 times, and homogenized in 1 ml of T-PER, Tissue Protein Extraction Reagent (Pierce, Rockford, IL, USA), containing 1% (v/v) proteinase inhibitor cocktail (Sigma-Aldrich, St Louis, MO, USA). The homogenates were clarified by centrifugation at 10,000g for 5 min at 4 °C. Protein content was measured using a BCA™ Protein Assay Kit (Pierce). The levels of IL-1α, IL-1β, IL-6, GM-CSF, G-CSF, TNFα, IFNγ, IL-15, MCP1, MIP1α, GRO/KC, and VEGF were measured by Multiplex Suspension array (GeneticLab, Co., Ltd., Sapporo, Japan).

### 2.7. Statistical analysis

Statistical analysis was performed using the Kruskal-Wallis and Bonferroni/Dunn's multiple comparison tests. The statistical significance was analyzed using a two tailed Student's *t*-test and the Bonferroni/Dunn's multiple comparison tests. A *P* value of <0.05 was considered to be significant.

## 3. Results

### 3.1. Size analysis of TiO<sub>2</sub> particles

The size (diameter) of TiO<sub>2</sub> particles suspended in Pentalan 408 ranged from 10 nm to 300 μm, with a mean size of 4.967 ± 0.500 μm and a median size of 4.570 μm, indicating that a large majority of the original nano-size (ultrafine grade) TiO<sub>2</sub> particles formed aggregates in the Pentalan 408 suspension (Fig. 2).

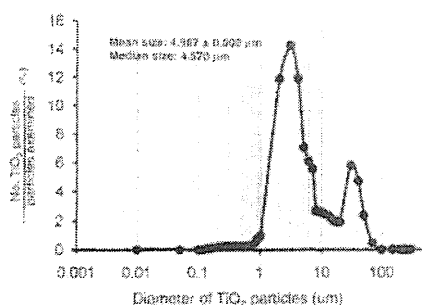


Fig. 2. Size distribution of  $\text{TiO}_2$  suspended in Pentalan 408. The size distribution of  $\text{TiO}_2$  particles suspended in Pentalan 408 was analyzed by a Particle Size Distribution Analyzer. The mean size was  $4.967 \pm 0.500 \mu\text{m}$  and the median size and  $4.570 \mu\text{m}$ .

### 3.2. Incidence of skin and mammary tumors

In male *Hras128* rats, papillomas on the back skin developed from week 32 and the incidence of skin papillomas was 1 out of 8 in Groups 1 and Group 3. No skin tumors were observed on the targeted back skin in female *Hras128* rats or wild-type rats of either sex. Eye lid squamous cell papillomas were found in wild-type female rats exposed to UVB (Groups 1 and 2) with incidences of 12.5% and 14.3% (Table 1). No statistically significant inter-group differences in incidence, multiplicity or weight were found (Table 1).

Mammary tumors, diagnosed as adenocarcinomas, were induced with high incidence in *Hras128* rats of both sexes. Wild-type female rats also had a relatively high incidence of mammary tumors compared with historical controls of spontaneous mammary tumor development. No statistically significant inter-group differences in incidence, multiplicity or weight were observed (Table 2).

### 3.3. Tissue analysis of $\text{TiO}_2$ particles

In the rat skin, no inflammatory lesions were observed by histopathological examination.  $\text{TiO}_2$  aggregates of various sizes were observed in the upper stratum corneum, but  $\text{TiO}_2$  was not found in the underlying epidermis, dermis or subcutaneous tissue (Fig. 3A). Some particles were found in the hair follicles at the level

Table 2  
Mammary tumors in *Hras128* and wild-type rats.

Sex	Group	Treatment	Incidence <sup>a</sup> (%)	Multiplicity <sup>b</sup> (No./rat)	Weight <sup>c</sup> (g/rat)
<i>Hras128</i>					
Male	1	UVB + $\text{TiO}_2$	4/8 (50)	$0.50 \pm 0.53$	$10.50 \pm 19.56$
	2	UVB	3/8 (36)	$0.38 \pm 0.51$	$10.17 \pm 17.69$
	3	$\text{TiO}_2$	4/8 (50)	$0.50 \pm 0.53$	$6.33 \pm 14.16$
Female	1	UVB + $\text{TiO}_2$	3/8 (83)	$1.67 \pm 1.37$	$11.48 \pm 20.61$
	2	UVB	2/5 (40)	$0.60 \pm 0.89$	$0.28 \pm 0.53$
	3	$\text{TiO}_2$	6/6 (100)	$1.33 \pm 0.52$	$4.49 \pm 9.76$
<i>Wild-type</i>					
Male	1	UVB + $\text{TiO}_2$	0/6	0	0
	2	UVB	0/5	0	0
	3	$\text{TiO}_2$	0/5	0	0
Female	1	UVB + $\text{TiO}_2$	1/8 (12.5)	$0.13 \pm 0.35$	$0.63 \pm 1.80$
	2	UVB	1/7 (14.3)	$0.14 \pm 0.38$	$0.71 \pm 1.93$
	3	$\text{TiO}_2$	0/8 (0)	0	0

<sup>a</sup> Rats died before sacrifice at week 52 were included.

of the granular cell layer in all the  $\text{TiO}_2$  treated groups, but not in the deeper parts of the hair follicles or in the surrounding tissue.

In the human epidermis model,  $\text{TiO}_2$  aggregates were observed only on the cornified layer of the epidermis, but not in the epidermis (Fig. 3B). The amount of elemental titanium in the receiving chamber did not show any significant difference from the vehicle alone group (Fig. 3C).

### 3.4. Cytokine analysis of the rat skin tissue

The levels of 12 inflammatory cytokines (IL-1 $\alpha$ , IL-1 $\beta$ , IL-6, GM-CSF, G-CSF, TNF $\alpha$ , IFN $\gamma$ , IL-18, MCP1, MIP1 $\alpha$ , GRO/JC, and VEGF) in the skin of rats receiving  $\text{TiO}_2$  treatment is shown in Table 3.  $\text{TiO}_2$  treatment did not have a significant effect on the expression of the cytokine levels in the skin compared with the vehicle group.

## 4. Discussion

$\text{TiO}_2$  particles, nano- and larger scale, are known to be carcinogenic to the rat lung (Baan et al., 2006), and the mechanism of lung carcinogenesis involves MIP1 $\alpha$  derived from  $\text{TiO}_2$ -laden alveolar macrophages (Xu et al., 2010). Thus, they are deemed to have the potential to cause skin tumors after long-term topical application,

Table 1  
Skin tumors in *Hras128* rats and wild-type rats.

Sex	Group	Treatment	Total No. of rats (died before termination)	Survival time (mean week $\pm$ SD)	Skin tumor <sup>a</sup>	
					Incidence (%)	Multiplicity (No./rat)
<i>Hras128</i>						
Male	1	UVB + $\text{TiO}_2$	8 (4 <sup>b</sup> )	$47.3 \pm 6.8$	1/8 (12.5)	$0.13 \pm 0.35$
	2	UVB	8 (4 <sup>b</sup> )	$48.4 \pm 5.5$	0/8	0
	3	$\text{TiO}_2$	8 (3 <sup>b</sup> )	$48.9 \pm 4.7$	1/8 (12.5)	$0.13 \pm 0.35$
Female	1	UVB + $\text{TiO}_2$	6	16	0/6	0
	2	UVB	5	16	0/5	0
	3	$\text{TiO}_2$	6	16	0/6	0
<i>Wild-type</i>						
Male	1	UVB + $\text{TiO}_2$	6	52	0/6	0
	2	UVB	5	52	0/5	0
	3	$\text{TiO}_2$	5	52	0/5	0
Female	1	UVB + $\text{TiO}_2$	8 (1 <sup>c,d</sup> )	$51.4 \pm 1.8$	1/8 (12.5)	$0.13 \pm 0.35$
	2	UVB	7 (1 <sup>c,d</sup> )	$51.4 \pm 1.5$	1/7 (14.3)	$0.14 \pm 0.38$
	3	$\text{TiO}_2$	8	52	0/8	0

<sup>a</sup> Rats died before sacrifice at week 52 were included in statistic calculation of the incidence and multiplicity.

<sup>b</sup> Rats died of mammary tumors between week 33 and week 51.

<sup>c</sup> Rats died of eye lid skin tumors during week 48 and week 50.

<sup>d</sup> Rats died of mammary tumors during week 48.



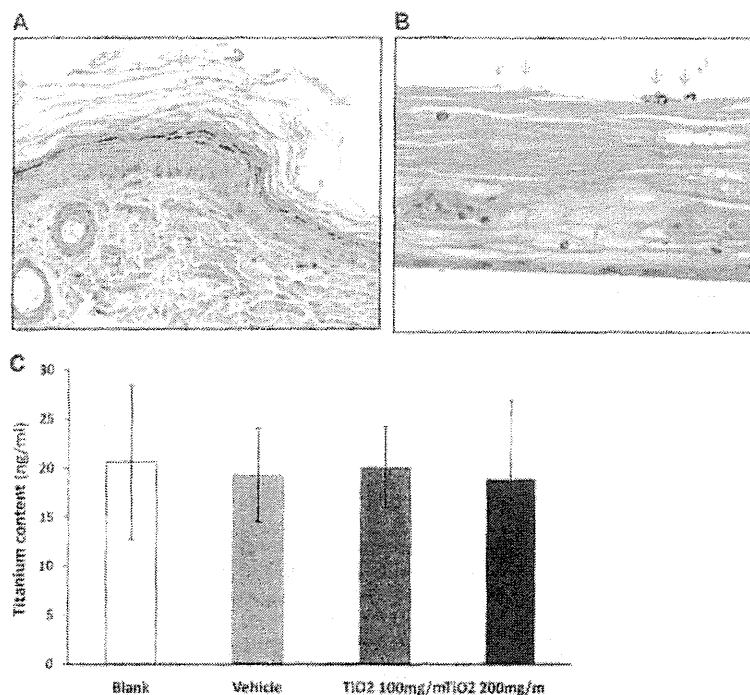


**Fig. 3.** TiO<sub>2</sub> particles did not penetrate the epidermis. (A) TiO<sub>2</sub> aggregates were observed in the upper stratum corneum, but were not found in the underlying epidermis, dermis or subcutaneous tissue. (B) In the *in vitro* penetration assay, TiO<sub>2</sub> aggregates were localized on the top of the human epidermis model, but not within the epidermis. (C) The amount of elemental titanium detected in the receiving chambers is expressed as mean  $\pm$  SD. A total of 24 wells of the epidermis model were exposed to the vehicle, 100 mg/ml or 200 mg/ml TiO<sub>2</sub> suspension. Arrows indicate TiO<sub>2</sub> aggregates.

**Table 3**  
Expression level of 12 inflammatory cytokines in the skin treated with Pentalan 408 or TiO<sub>2</sub> (5 rats in each group, ng/mg protein)

Cytokine	Pentalan 408	TiO <sub>2</sub> suspension
GM-CSF	23.65 $\pm$ 36.48	23.01 $\pm$ 16.75
G-CSF	0.37 $\pm$ 0.21	0.13 $\pm$ 0.16
IL-1 $\alpha$	2914 $\pm$ 433	3176 $\pm$ 785
IL-1 $\beta$	39.81 $\pm$ 7.49	30.87 $\pm$ 7.26
IL-6	1.33 $\pm$ 2.97	0.00 $\pm$ 0.00
TNF $\alpha$	29.56 $\pm$ 7.75	26.00 $\pm$ 8.07
INF $\gamma$	5.91 $\pm$ 0.68	4.70 $\pm$ 1.10
IL-18	845 $\pm$ 234	763 $\pm$ 299
MCP-1	90 $\pm$ 125	123 $\pm$ 125
MIP-1 $\alpha$	3.47 $\pm$ 7.75	0.00 $\pm$ 0.00
GRO/KC	82.66 $\pm$ 21.86	63.04 $\pm$ 28.76
VEGF	17.96 $\pm$ 19.05	14.04 $\pm$ 17.65

especially if they induce inflammatory lesions including enhanced macrophage activity in the skin. The present study is the first report of an *in vivo* skin promotion/carcinogenesis study of TiO<sub>2</sub> particles topically applied to the back skin of rats. The incidence of skin tumors in male Hras128 was 1 out of 8 (12.5%) in the TiO<sub>2</sub> alone group and in the UVB plus TiO<sub>2</sub> group, higher than that of spontaneously developed skin tumors in these rats (less than 5%) (Park et al., 2004). However, no inter-group difference was observed. Our results demonstrate that TiO<sub>2</sub> suspension does not have a promoting effect on skin carcinogenesis after UVB radiation.

The lack of skin carcinogenesis promotion activity is probably due to lack of penetration of TiO<sub>2</sub> particles through the epidermis to the dermis, where skin tumors arise. Histologically, topically applied TiO<sub>2</sub> particles were located only in the upper stratum corneum and in some hair follicles at the level of granular cell layer, but were not found in the epidermis or the underlying dermis.

Our results are consistent with other reports (Mavon et al., 2007; Pflucker et al., 2001). Furthermore, results of the *in vitro* skin model assay used in our study indicate that TiO<sub>2</sub> particles do not penetrate the human epidermis. Since the size of TiO<sub>2</sub> particles was a mixture of nano-size and micro-size, the results indicate that overall the particles do not penetrate through the epidermis and cause an inflammatory response in the skin, although a trace amount of nano-size particles might penetrate the skin tissue. In our study, a large majority of the original nano-size TiO<sub>2</sub> particles (ultrafine grade) formed micro-size aggregates in the Pentalan 408 suspension and this may have affected the particle penetration. The difference between the report of Wu et al. (2009) and ours *in vivo* observation may be ascribed to different test animals, different TiO<sub>2</sub> particles used or different methods of making the TiO<sub>2</sub> particle suspension.

The high incidence of mammary tumors Hras128 rats regardless of treatment is attributed to spontaneous development, which is specific to the Hras128 rat (Asamoto et al., 2000; Matsuoka et al., 2007; Tsuda et al., 2005).

TiO<sub>2</sub> particle-induced lung carcinogenesis in rats is due to chronic inflammation (ILSI, 2000) with the cytokine MIP1 $\alpha$ , derived from TiO<sub>2</sub>-laden alveolar macrophages, being an important mediator of carcinogenesis (Xu et al., 2010). In the present study, analysis of 12 inflammatory cytokines, IL-1 $\alpha$ , IL-1 $\beta$ , IL-6, GM-CSF, G-CSF, TNF $\alpha$ , INF $\gamma$ , IL-18, MCP1, MIP1 $\alpha$ , GRO/KC, and VEGF, indicated that no significant change in the expression level of these cytokines occurred after topical application of TiO<sub>2</sub>. This result, together with histological observation, indicates that no inflammatory reaction is evoked by topical application of TiO<sub>2</sub>. This may partly explain why topical application of TiO<sub>2</sub> suspension has no carcinogenic effect in the skin.

Since tumor promotion activity is considered to be a weak carcinogenic activity (IARC, 1980; Ito et al., 1988, 2003; Konishi et al.,

1987; Nishikawa et al., 1994; Peraino et al., 1971; Pitot et al., 1978; Yamanaka et al., 1996), lack of promotion activity can be interpreted as lack of carcinogenic activity. Thus, the results of our present study indicate that topical application of TiO<sub>2</sub> suspension does not have carcinogenic activity on UVB-treated skin in rats, probably due to lack of penetration through the epidermis. In conclusion, our results indicate that topical application of TiO<sub>2</sub> can be considered to be safe and not carcinogenic to the skin or other organs.

## 5. Conflict of Interest

The authors declare that there are no conflicts of interest.

## Acknowledgement

This work was supported by Health and Labour Sciences Research Grants (Research on Risk of Chemical Substance, H19-kagaku-ippan-006 and H22-kagaku-ippan-005), and Grant-in aid for cancer research from the Ministry of Health, Labour and Welfare, Japan, a grant-in-aid for the Second Term Comprehensive 10-year Strategy for Cancer Control from the Ministry of Health, Labour and Welfare, Japan, and grants-in aid for Cancer Research from the Ministry of Education, Culture, Sports, Science and Technology. Jieyou Xu was a recipient of Bantane Houtokukai Fellowship when this study was performed.

## References

- Anderson, M., Hewitt, J., Spruce, J., 1997. Broad-spectrum physical sunscreen: titanium dioxide and zinc oxide. In: Lowe, N.J., Shaath, N.A., MA, P. (Eds.), *Sunscreens: Development, Evaluation and Regulatory Aspects*, New York: Dekker, pp. 357–397.
- Asamoto, M., Ochiya, T., Tonyama-Baba, H., Ota, T., Sekiya, T., Terada, M., Tsuda, H., 2000. Transgenic rats carrying human c-Ha-ras proto-oncogenes are highly susceptible to N-methyl-N-nitrosourea mammary carcinogenesis. *Carcinogenesis* 21, 243–249.
- Baan, R., Straif, K., Grosse, Y., Secretan, B., El Ghissassi, F., Coghiano, V., 2006. Carcinogenicity of carbon black, titanium dioxide, and talc. *Lancet Oncol.* 7, 295–296.
- Baroli, B., Ennas, M.G., Loffredo, F., Isola, M., Pinna, R., Lopez-Quintela, M.A., 2007. Penetration of metallic nanoparticles in human full-thickness skin. *J. Invest. Dermatol.* 127, 1701–1712.
- Celis, C., Girard, S., Mavon, A., Deverdier, M., Pailhoux, N., Vicendo, P., 2003. Assessment of the skin photoprotective capacities of an organo-mineral broad-spectrum sunblock on two ex vivo skin models. *Photodermatol. Photoimmunol. Photomed.* 19, 242–253.
- Gottbrath, S., Müller-Coymann, C.C., 2003. Penetration and visualization of titanium dioxide microparticles in human stratum corneum—effect of different formulations on the penetration of titanium dioxide. *SOPW J.* 129, 11–17.
- IARC (1980). Long-term and short-term screening assays for carcinogens: a critical appraisal. 1980/01/01 edn).
- ILSI. 2000. The relevance of the rat lung response to particle overload for human risk assessment: a workshop consensus report. ILSI Risk Science Institute Workshop Participants. *Inhal. Toxicol.* 12, 1–17.
- ISO (2006). Nanotechnologies—Terminology and definition for nano-object—nanoparticle, nanofibre and nanoplate. ISO/TS 27687.
- Ito, N., Inaida, K., Tsuda, H., Shibata, M., Aoki, T., de Camargo, J.L., Fukushima, S., 1988. Wide-spectrum initiation models: possible applications to medium-term multiple organ bioassays for carcinogenesis modifiers. *Jpn. J. Cancer Res.* 79, 413–417.
- Ito, M., Tamano, S., Shirai, T., 2003. A medium-term rat liver bioassay for rapid in vivo detection of carcinogenic potential of chemicals. *Cancer Sci.* 94, 3–8.
- Kim, S., Lim, Y.T., Softes, E.G., De Grand, A.M., Lee, J., Nakayama, A., Parker, J.A., Mihajevic, T., Laurence, R.G., Dor, D.M., Cohn, L.H., Bawendi, M.G., Frangioni, J.V., 2004. Near-infrared fluorescent type II quantum dots for sentinel lymph node mapping. *Nat. Biotechnol.* 22, 93–97.
- Konishi, Y., Yokose, Y., Mori, Y., Yamazaki, H., Yamamoto, K., Nakajima, A., Denda, A., 1987. Lung carcinogenesis by N-nitroso bis(2-hydroxypropyl)amine-related compounds and their formation in rats. *IARC Sci. Publ.* 1, 250–252.
- Lee, K.P., Trochimowicz, H.J., Reinhardt, C.F., 1985. Pulmonary response of rats exposed to titanium dioxide (TiO<sub>2</sub>) by inhalation for two years. *Toxicol. Appl. Pharmacol.* 79, 179–192.
- Matsuoka, Y., Kawaguchi, H., Yoshida, H., Tsuda, H., Tsubura, A., 2007. Rat mammary preneoplasia and neoplasia: a model for human breast cancer research. *Trends Cancer Res.* 3, 1–13.
- Mavon, A., Miquel, C., Lejeune, O., Payre, B., Moretto, P., 2007. In vitro percutaneous absorption and in vivo stratum corneum distribution of an organic and a mineral sunscreen. *Skin Pharmacol. Physiol.* 20, 10–20.
- Newman, M.D., Stotland, M., Ellis, J.L., 2008. The safety of nano-sized particles in titanium dioxide- and zinc oxide-based sunscreens. *J. Am. Acad. Dermatol.* 61, 685–692.
- Nishikawa, A., Furukawa, F., Imazawa, T., Yoshimura, H., Ikezaki, S., Hayashi, Y., Takahashi, M., 1994. Effects of cigarette smoke on N-nitrosobis(2-oxopropyl)amine-induced pancreatic and respiratory tumorigenesis in hamsters. *Jpn. J. Cancer Res.* 85, 1000–1004.
- Nohynek, G.J., Dufour, E.K., Roberts, M.S., 2008. Nanotechnology, cosmetics and the skin: is there a health risk? *Skin Pharmacol. Physiol.* 21, 136–149.
- Park, C.B., Fukamachi, K., Takasuka, N., Han, B.S., Kim, C.K., Hamaguchi, T., Fujita, K., Ueda, S., Tsuda, H., 2004. Rapid induction of skin and mammary tumors in human c-Ha-ras proto-oncogene transgenic rats by treatment with 7, 12-dimethylbenz[*a*]anthracene followed by 12-O-tetradecanoylphorbol 13-acetate. *Cancer Sci.* 95, 205–210.
- Peraino, C., Fry, R.J., Staffeldt, E., 1971. Reduction and enhancement by phenobarbital of hepatocarcinogenesis induced in the rat by 2-acetylaminofluorene. *Cancer Res.* 31, 1506–1512.
- Peters, K., Unger, R.E., Kirkpatrick, C.J., Gatti, A.M., Monari, E., 2004. Effects of nano-sized particles on endothelial cell function in vitro: studies on viability, proliferation and inflammation. *J. Mater. Sci.: Mater. Med.* 15, 321–325.
- Pflucker, F., Wendel, V., Hohenberg, H., Gartner, E., Will, T., Pfeiffer, S., Wepf, R., Gers-Barlag, H., 2001. The human stratum corneum layer: an effective barrier against dermal uptake of different forms of topically applied micronized titanium dioxide. *Skin Pharmacol. Appl. Skin Physiol.* 14 (Suppl. 1), 92–97.
- Pitot, H.C., Barnes, L., Goldworthy, T., Kitagawa, Y., 1978. Biochemical characterization of stages of hepatocarcinogenesis after a single dose of diethylnitrosamine. *Nature* 271, 456–458.
- Pott, F., Rofler, M., 2005. Carcinogenicity study with nineteen granular dusts in rats. *Eur. J. Oncol.* 10, 249–281.
- Rouabhi, M., Mitchell, D.L., Rhoads, M., Claveau, J., Drouin, R., 2002. A physical sunscreen protects engineered human skin against artificial solar ultraviolet radiation-induced tissue and DNA damage. *Photochem. Photobiol. Sci.* 1, 471–477.
- Suzuki, M., 1967. Protective effect of fine-particle titanium dioxide on UVB-induced DNA damage in hairless mouse skin. *Photodermatology* 4, 209–211.
- Tsuda, H., Fukamachi, K., Ohshima, Y., Ueda, S., Matsuoka, Y., Hamaguchi, T., Ohnishi, T., Takasuka, N., Naito, A., 2005. High susceptibility of human c-Ha-ras proto-oncogene transgenic rats to carcinogenesis: a cancer-prone animal model. *Cancer Sci.* 96, 309–316.
- Wu, J., Liu, W., Xue, C., Zhou, S., Lan, F., Bi, L., Xu, H., Yang, X., Zeng, F.D., 2009. Toxicity and penetration of TiO<sub>2</sub> nanoparticles in hairless mice and porcine skin after subchronic dermal exposure. *Toxicol. Lett.* 191, 1–8.
- Xu, J., Futakuchi, M., Iigo, M., Fukamachi, K., Alexander, D.B., Shimizu, H., Sakai, Y., Tamano, S., Furukawa, F., Uchino, T., Tokunaga, H., Nishimura, T., Hirose, A., Kanno, J., Tsuda, H., 2010. Involvement of macrophage inflammatory protein 1alpha (MIP1alpha) in promotion of rat lung and mammary carcinogenic activity of nanoscale titanium dioxide particles administered by intrapulmonary spraying. *Carcinogenesis* 31, 927–935.
- Yamanaka, K., Ohtsubo, K., Hasegawa, A., Hayashi, H., Ohji, H., Kanisawa, M., Okada, S., 1996. Exposure to dimethylarsinic acid, a main metabolite of inorganic arsenites, strongly promotes tumorigenesis initiated by 4-nitroquinoline 1-oxide in the lungs of mice. *Carcinogenesis* 17, 767–770.

RESEARCH ARTICLE

Open Access

# A Cross-Species Analysis of a Mouse Model of Breast Cancer-Specific Osteolysis and Human Bone Metastases Using Gene Expression Profiling

Anguraj Sadanandam<sup>1,6\*</sup>, Mitsuru Futakuchi<sup>2</sup>, Costas A Lyssiotis<sup>3,4</sup>, William J Gibb<sup>5</sup> and Rakesh K Singh<sup>1\*</sup>

## Abstract

**Background:** Breast cancer is the second leading cause of cancer-related death in women in the United States. During the advanced stages of disease, many breast cancer patients suffer from bone metastasis. These metastases are predominantly osteolytic and develop when tumor cells interact with bone. *In vivo* models that mimic the breast cancer-specific osteolytic bone microenvironment are limited. Previously, we developed a mouse model of tumor-bone interaction in which three mouse breast cancer cell lines were implanted onto the calvaria. Analysis of tumors from this model revealed that they exhibited strong bone resorption, induction of osteoclasts and intracranial penetration at the tumor bone (TB)-interface.

**Methods:** In this study, we identified and used a TB microenvironment-specific gene expression signature from this model to extend our understanding of the metastatic bone microenvironment in human disease and to predict potential therapeutic targets.

**Results:** We identified a TB signature consisting of 934 genes that were commonly (among our 3 cell lines) and specifically (as compared to tumor-alone area within the bone microenvironment) up- and down-regulated >2-fold at the TB interface in our mouse osteolytic model. By comparing the TB signature with gene expression profiles from human breast metastases and an *in vitro* osteoclast model, we demonstrate that our model mimics both the human breast cancer bone microenvironment and osteoclastogenesis. Furthermore, we observed enrichment in various signaling pathways specific to the TB interface; that is, TGF- $\beta$  and myeloid self-renewal pathways were activated and the Wnt pathway was inactivated. Lastly, we used the TB-signature to predict cyclopenthiiazide as a potential inhibitor of the TB interface.

**Conclusion:** Our mouse breast cancer model morphologically and genetically resembles the osteoclastic bone microenvironment observed in human disease. Characterization of the gene expression signature specific to the TB interface in our model revealed signaling mechanisms operative in human breast cancer metastases and predicted a therapeutic inhibitor of cancer-mediated osteolysis.

**Keywords:** Osteolysis, bone metastasis, tumor-bone microenvironment, thiazide

## Background

Bone is one of the most common sites for metastasis in human breast cancer. Bone metastasis results in cancer-related pain, pathological fracture, hypercalcemia, neurological defects, and immobility; all of which increase the risk of mortality and decrease the quality of life for breast

cancer patients [1-4]. While a number of strategies exist to treat breast cancer bone metastases (e.g., surgery, radiation and/or chemotherapy), none are curative. Furthermore, these treatment methods have limited efficacy due in part to the fact that they do not effectively target the interaction between tumor cells and bone [5]. Even though the bisphosphonate class of drugs (which target the tumor-bone interface) have been shown to improve the quality of life and disease-free survival in

\* Correspondence: anguraj.sadanandam@epfl.ch; rsingh@unmc.edu

<sup>1</sup>Department of Pathology and Microbiology, University of Nebraska Medical Center, Omaha, NE 68198-5900, USA

Full list of author information is available at the end of the article

some patients, more therapeutic targets and agents are desirable [6].

Within the osteolytic lesions of bone metastases, tumor cells interact with osteoclasts (bone resorbing cells) and osteoblasts (bone forming cells), thereby inhibiting normal bone development and ultimately leading to bone destruction [1-4]. As for osteoclasts, their interaction with tumor cells is reciprocal: tumor cells produce factors (e.g., parathyroid hormone-related peptide; interleukin-6; tumor necrosis factor; and macrophage colony stimulating factor, M-CSF) that directly or indirectly induce the formation of osteoclasts, and activated osteoclasts produce factors (e.g., transforming growth factor, TGF- $\beta$ ; insulin growth factor, IGF; and bone morphogenetic proteins, BMPs) that stimulate tumor growth and bone destruction [1]. Despite a general comprehension of this process, we are still far from a complete mechanistic understanding and lack well defined targets for therapeutic intervention.

Several animal models have been developed to study the mechanisms governing cancer-mediated osteolysis. However, there is no single animal model that ideally replicates the entire metastatic process from primary breast tumor to bone metastasis. Nevertheless, several models that represent various aspects of bone metastasis have been used successfully to study specific features of the disease. For example, Arguello, et al. developed a model in which melanoma cells injected into the left ventricle of the heart ultimately form bone metastases [7]. This model was later used to study various mechanisms behind breast cancer-specific osteoclast formation and bone metastasis [8-10]. Our group has also developed a rat model to study bone metastatic microenvironment in which prostate tumors were directly transplanted onto the calvariae of syngeneic animals. These tumors exhibited pathological osteoblastic and osteoclastic changes [11]. More recently, we used this approach with mouse breast cancer cell lines and found that the tumor cells induce osteolytic changes in the bone microenvironment [12-15]. With this model, we found that cathepsin G cleaves the receptor activator of nuclear factor- $\kappa$ B ligand (Rankl) leading to enhanced activation of osteoclasts in the breast cancer bone microenvironment [15]. Furthermore, we also demonstrated the importance of TGF- $\beta$  signaling and osteoclast activation in the breast cancer bone microenvironment [12,14]. While this series of observations has furthered our understanding of the mechanisms underlying osteolysis, their relevance to human breast cancer remained unknown.

To address this question, we reanalyzed gene expression profiles generated from our previous studies using the syngeneic mouse model of breast cancer specific osteolysis that was developed by implanting 3 different cell lines - 4T1 (highly metastatic), Cl66 (moderately

metastatic) and Cl66-M2 (low metastatic) - onto the calvariae bone of BALB/C mice [12-15]. The gene expression profiles were generated from microdissected tumors in which the tumor-bone (TB) interface and the tumor alone (TA) area were isolated independently. Then we identified a TB signature involved in bone destruction by comparing the gene expression profiles of the TA area and TB interface from the dissected tumors. Lastly, using our TB signature, open-access gene expression data, and pathway analytics, we demonstrated that our model mimics human disease and predicted key pathways and a potential therapeutic agent for breast cancer osteolysis.

## Methods

### Mouse osteolytic model and microarray

Mouse breast cancer cell lines - 4T1, Cl66 (66Cl4) and Cl66M2 - with different metastatic potential [16-18] were maintained in culture and were implanted under the dorsal skin flap onto the calvaria of female BALB/c mice, as described [12]. Mice were euthanized and necropsied to examine osteolytic lesions at 4 weeks post implantation. The tissues for histological examination were prepared as described [12]. All studies were carried out in accordance with the Institutional Animal Use and Care Committee (IAUCC) of the University of the Nebraska Medical Center. Calcified frozen tissues were serially sectioned into 10  $\mu$ m slices and then microdissected to separate the TB interface from the TA area. RNA isolation and gene expression profiling of the TB interface and TA area were performed using Affymetrix GeneChip<sup>®</sup> Mouse Genome 430A 2.0 Array, as described [14].

### Analysis of gene arrays and public microarray datasets

The CEL files for all the samples from Affymetrix GeneChip<sup>®</sup> were processed and MAS 5.0-normalized using the SimpleAffy [19] program and robust multiarray (RMA)-normalized using BRB Array tools [20]. The log<sub>2</sub> MAS 5.0-normalized data was used for subsequent analyses. Fold-change at the TB interface with respect to the TA area for tissues, standard deviation (SD) across TA samples, and median-centered analysis within the TA area were calculated for each of the cell lines (4T1, Cl66 and Cl66-M2) to identify genes up- and down-regulated in the respective samples. The genes were ranked from highest to lowest expression based on the values from fold-change or median-centered analysis.

The following publicly available Affymetrix microarray data were obtained from Gene Expression Omnibus (GEO) [21]: GSE13563 for normal bone from mouse calvaria (n = 2), mandible (n = 2) and ulna (n = 2); GSE14017 (n = 29) and GSE14018 (n = 36) for metastases from breast cancer [22]; GSE11259 (n = 9) for 4T1 primary tumor data [23]; and GSE17563 (n = 3) for osteoclast precursors treated with human RANKL at different time

points [24]. All the GEO data were processed and normalized as described above. Affymetrix microarray data for breast tumors (n = 118) [25] and cancer cell lines (n = 54) [26] were also compared with the TA area gene expression profile.

The NearestTemplatePrediction algorithm (NTP) [27,28] was used to predict the class of a given sample with statistical significance (false discovery rate, FDR < 0.2) using a predefined set of markers that are specific to multiple classes (TB interface vs. TA area). Microarray data from different studies and platforms were sample- and gene-normalized and then pooled using the Distance Weighted Discrimination (DWD) algorithm, as described [29,30]. The significance of expression between the mouse model and human bone metastases was estimated using SubMap [31]. Hierarchical clustering of genes and samples were performed using the Cluster software [32]. Visualization was performed with TreeView [32] and Hierarchical Clustering Viewer from GenePattern [33].

#### Gene ontology (GO) and pathway analysis

The association of gene signature with known pathways was determined using gene ontology (GO) [34], pathways from Kyoto Encyclopedia of Genes and Genomes (KEGG) [35], and Broad Institute based Molecular Signature Databases (MSigDB) [36]. The enrichment analysis was performed using the TB signature and the GlobalTest package (Version 4.2.0) [37,38].

#### Connectivity Map analysis

Gene symbols were mapped to HG-U133A array probes. They were then used to query the Connectivity Map database [39].

## Results

#### The TA area resembles the primary tumor

Previously, we transplanted three breast cancer cell lines - 4T1 (highly metastatic), Cl66 (moderately metastatic) and Cl66-M2 (low metastatic) - onto the calvarial bone of BALB/C mice [12,14]. Irrespective of the cell lines used, histochemical analysis of these tumors demonstrated that they exhibited tumor-induced osteolysis and osteoclast activation similar to that observed in breast cancer bone metastasis [12,14]. Metastatic lesions from the osteolytic tumors were microdissected into two cohorts - TB interface and TA area - and gene expression profile analyses were performed [12,14]. Herein, we reanalyzed these gene expression data sets in search of a breast cancer osteolysis-specific gene signature.

Our reanalysis illustrates that there is little similarity in gene expression in the TA area samples among the three cell lines (Figure 1A). This is altogether not too surprising given that these cell lines were originally derived from different mouse tumors [16-18]. Consistently, the

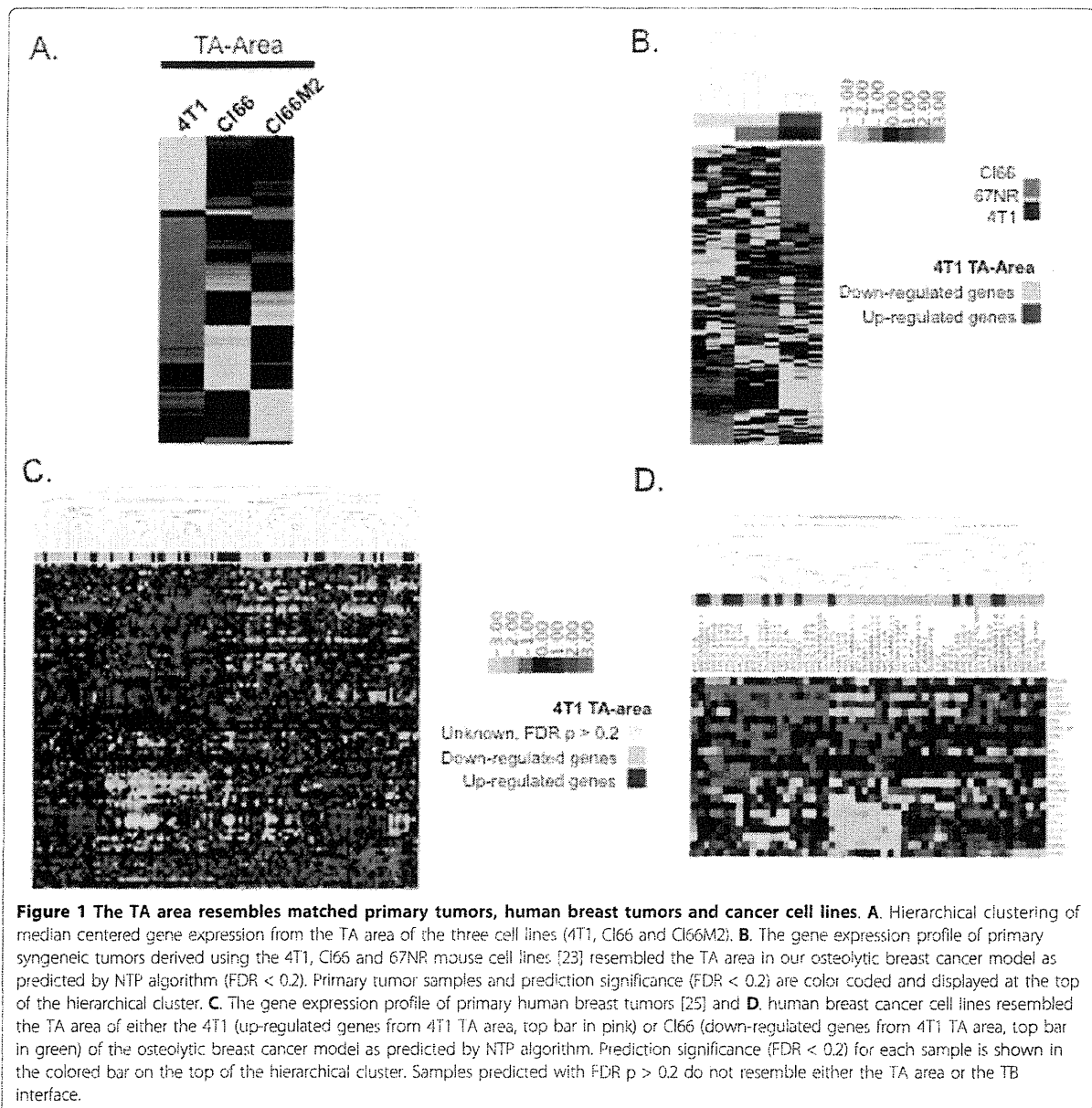
sublines Cl66 and Cl66-M2 [16-18], share the most similarity in gene expression (Figure 1A).

The TA area was grown in a non-canonical tumor microenvironment (i.e., bone instead of breast) and as such can be considered a metastatic tumor. Nevertheless, we still expect that the gene expression profile from the TA area (grown near bone) will resemble previously reported profiles for the cell lines (grown in the breast) used in this study, especially given the fact that the primary tumor and its metastatic tumor have been reported to have similar gene expression profiles [40]. To confirm that the TA area expression signature of each cell line resembles that of primary tumors, we used a public gene expression profile of tumors grown in the breast from the 4T1 and Cl66 (66Cl4) cell lines [23]. Reassuringly, the up-regulated genes from the TA area of 4T1 cells significantly (FDR  $p < 0.2$ ) predicted primary tumors from 4T1 cells and the down-regulated genes predicted tumors from Cl66 using the NTP algorithm (Figure 1B). Since the gene signature from the TA area of 4T1 cells are reported relative to Cl66 and Cl66-M2, most of the down-regulated genes represent those up-regulated in Cl66 and Cl66-M2. These results demonstrate that the gene expression profile from our microdissected TA area samples represents that of primary tumors.

In an effort to translate our findings from our mouse breast tumor model to human disease, we compared the gene expression profile from the TA area of our mouse model to that of primary human breast tumors and cancer cell lines using the NTP algorithm. Specifically, we compared microarray data from 118 primary breast tumor samples [25] to the gene expression profile from the 4T1 and Cl66 TA areas. Interestingly, 37 breast tumor samples (top bar in pink) were significantly associated with 4T1 TA area and 34 breast tumor samples were significantly associated with Cl66 TA area (top bar in green) with an FDR  $p < 0.2$  (Figure 1C). Our analysis also predicted that 16 (top bar in pink) and 3 (top bar in green) out of 54 human breast cancer cell lines [26] resemble 4T1 and Cl66 tumors, respectively (Figure 1D). Again, the down-regulated TA area genes represent the TA area of Cl66 and Cl66-M2. This analysis predicts that it is possible to use these 19 human breast cancer cell lines in our mouse model and that similar results could be obtained.

#### TB interface-specific gene expression signature

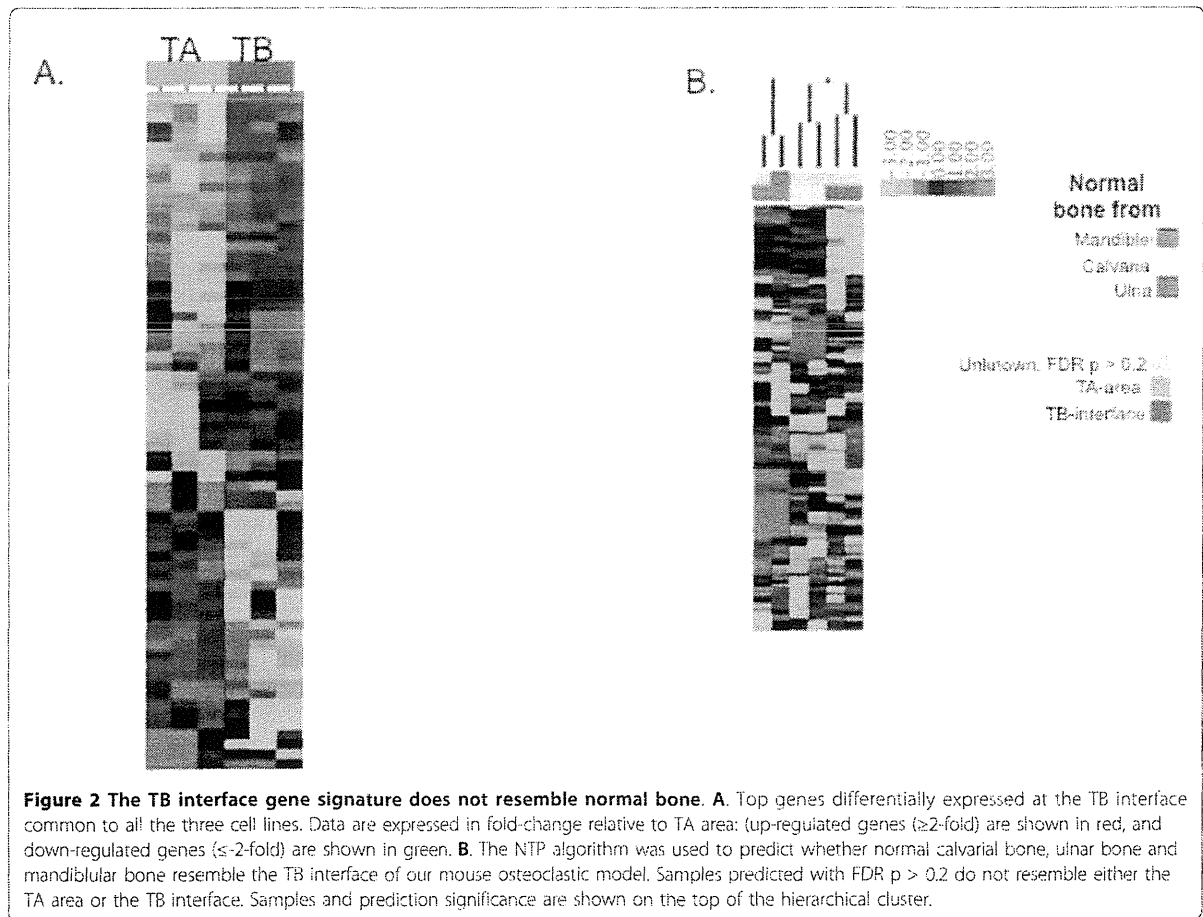
In order to identify genes that are important for the interaction of breast cancer cells with the tumor microenvironment, we reanalyzed the gene expression at the TB interface and compared that profile to the gene expression profile at the TA area for each of the cell lines. Despite the expected heterogeneity in gene expression from cell line to cell line, we were able to identify 934 genes (TB signature) that were consistently different between the TB



interface and the TA area. Among these, 359 were up-regulated and 575 were down-regulated with at least a 2-fold change at the TB interface across all the three cell lines. Figure 2A illustrates the top 50 known up- and down-regulated genes. The top differentially expressed genes are detailed in Tables 1 and 2.

The gene expression profile of the TB interface was identified relative to the TA area, and, as such, should be enriched for transcriptional processes associated with the TB microenvironment. Indeed, three of the top four genes up-regulated at the TB interface (i.e., receptor activator of

NF- $\kappa$ B ligand, Rankl; integrin binding sialoprotein, Ibsp; and matrix metalloproteinase 13, Mmp13) are well established as mediators of bone metastasis [7,11-13,15,41,42]. Table 1 highlights the fold-change of these genes at the TB interface as compared to the TA area (from the Affymetrix microarray profiling). Furthermore, we have previously validated the expression and function of several of these genes in our mouse model [12-15]. Collectively, these data strongly suggest that our analysis identified genes uniquely enriched in and important for the metastatic bone microenvironment.



**The TB microenvironment is different than normal bone**  
 Next, we compared the specificity of our TB specific gene set against that from the normal bone microenvironment. To this end, we used a public gene expression profile containing data for normal mouse calvarial bone, normal mouse ulnar bone and normal mouse mandibular bone (GSE13563). Our TB signature was compared

against this data set using the NTP algorithm. As shown in Figure 2B, none of the calvarial or ulnar samples are enriched for the TB-signature (FDR  $p > 0.2$ ), though one of the mandibular bone samples is predicted to be similar to TB microenvironment. This data demonstrates that the TB interface is genetically different from the microenvironment of normal bone.

**Table 1 Genes up-regulated in the TB interface and their fold-change relative to the TA area**

Gene	Affymetrix probe ID	Description	Fold change	p-value	FDR p-value
Ibsp	1417484_at or 1417485_at	Integrin binding sialoprotein	7.2	0.05	0.2
Tnfrsf11 (Rankl)	1419083_at or 1451944_a_at	Tumor necrosis factor (ligand) superfamily, member 11	5.3	0.005	0.1
Aftph	1426861_at	Afitiphilin	4.8	0.05	0.2
Mmp13	1417256_at	Matrix metalloproteinase 13	4.7	0.05	0.2
Anks1b	1447464_at	Ankyrin repeat and sterile alpha motif domain containing 1B	4.4	0.02	0.1
Zic1	1423477_at or 1439627_at	Zinc finger protein of the cerebellum 1	3.7	0.09	0.2
Drd1a	1455629_at or 1456051_at	Dopamine receptor 1A	3.6	0.005	0.1
Alpk2	1452478_at	Alpha-kinase 2	3.2	0.005	0.1
Smoc2	1415935_at or 1431362_a_at	SPARC related modular calcium binding 2	3.2	0.01	0.1

**Table 2 Genes down-regulated in the TB interface and their fold-change relative to the TA area**

Gene	Affymetrix probe ID	Description	Fold change	p-value	FDR p-value
Cnpy1	1437996_s_at	Canopy 1 homolog (Zebrafish)	-5.0	0.09	0.2
Adora3	1429609_at or 1430482_at	Adenosine A3 receptor	-4.7	0.04	0.2
Tmco5	1420341_at	Transmembrane and coiled-coil domains 5	-4.5	0.1	0.2
Vlra2	1427675_at	Vomerolnasal 1 receptor, A2	-4.4	0.07	0.2
Maf	1435828_at	Avian musculoaponeurotic fibrosarcoma (v-maf) A542 oncogene homolog	-3.9	0.02	0.1
Dll3	1449236_at	Delta-like 3	-2.9	0.04	0.2
Krtap16-1	1425655_at	Keratin associated protein 16-1	-2.9	0.01	0.1
Camta1	1433971_at	Calmodulin binding transcription activator 1	-3.5	0.01	0.1

### The TB interface resembles the metastatic bone microenvironment of human breast cancer

A primary concern with any animal model is whether it accurately represents human disease. To address this, we applied NTP using the TB signature and publicly available gene expression profiles of human breast metastases (i.e., brain, lung and bone) [22]. As shown in Figure 3A, 60% of the samples from bone metastases were significantly predicted (FDR  $p < 0.2$ ) to belong to the TB interface of our model. Importantly, the gene expression profiles of metastases from both brain and lung did not correlate with the TB interface data.

In addition, we also performed the Gene Set Enrichment Analysis (GSEA) [36] based SubMap algorithm [31] to predict if the TB interface gene expression profile resembles bone metastases from humans. Here, SubMap analysis with the TB signature was used to compare different human metastases samples (brain, bone and lung) to the sample sets from our mouse model (TB interface and TA area). Interestingly, *de novo* analysis showed that TB interface samples significantly (FDR  $< 0.2$ ) resemble bone metastases samples but not lung or brain samples. TA area samples also do not resemble any of the metastases (Figure 3B). Furthermore, the Rankl and Mmp13 genes, which are up-regulated at the TB interface, are also up-regulated in the human bone metastases samples. Collectively, these data demonstrate that the osteolytic bone microenvironment in our mouse model mimics the bone microenvironment in human breast cancer but not that of other metastatic microenvironments (i.e., lung and brain metastases).

### The TB interface resembles osteoclastogenesis in culture

The Rankl-mediated differentiation of osteoclast precursors (OCPs) to mature osteoclasts is a key step in breast cancer-specific bone metastasis [43]. Since Rankl is among the most highly up-regulated genes at the TB interface, we suspected that osteoclastogenesis may be

occurring at the TB interface in our mouse model. To address this possibility, we performed NTP analysis using our TB signature and a publicly available gene expression profile from OCPs that have been differentiated into osteoclasts *in vitro* [24]. The osteoclasts used in the aforementioned data set were generated following a two stage differentiation protocol: OCPs were pretreated with macrophage colony stimulating factor (M-CSF) and then treated with human RANKL for 0, 24 or 72 h. Terminal osteoclast differentiation requires at least 72 h of RANKL treatment [24]. NTP analysis of our TB signature predicted that it was similar to OCPs treated with RANKL for 72 h with a FDR of  $p = 0.2$ . Interestingly, our TB signature did not correlate with either RANKL-untreated OCPs or those only treated for 24 h (Figure 3C). This analysis suggests that osteoclastogenesis is occurring at the TB interface in our model.

### Pathways associated with the TB interface

To assess whether mechanisms that govern bone metastasis in humans are also present in our osteolytic model, we performed Gene Ontology (GO) [34]; pathway Kyoto Encyclopedia of Genes and Genomes, KEGG [44]; and Broad Institute based Molecular Signature Databases, MSigDB [45] canonical pathway enrichment analysis. The enrichment analysis was performed using the TB signature and the GlobalTest package [37,38]. Table 3 shows GO terms significantly (FDR  $p < 0.05$ ) associated with our osteolytic model. Among the GO terms significantly associated with the TB signature is TGF- $\beta$  signaling (Figure 4A). Indeed, the TGF- $\beta$  superfamily ligand Bmp10 is up-regulated at the TB interface in all three cell lines (greater than 2-fold in C166 and C166M2; data not shown). This would suggest that TGF- $\beta$  superfamily signaling is mediated in part by the Bmp10 ligand in our model. Consistently, negative regulators (Sostdc1 and Cer1) of the TGF- $\beta$  pathway are down-regulated at the TB interface and up-regulated in TA area (Figure 4A).



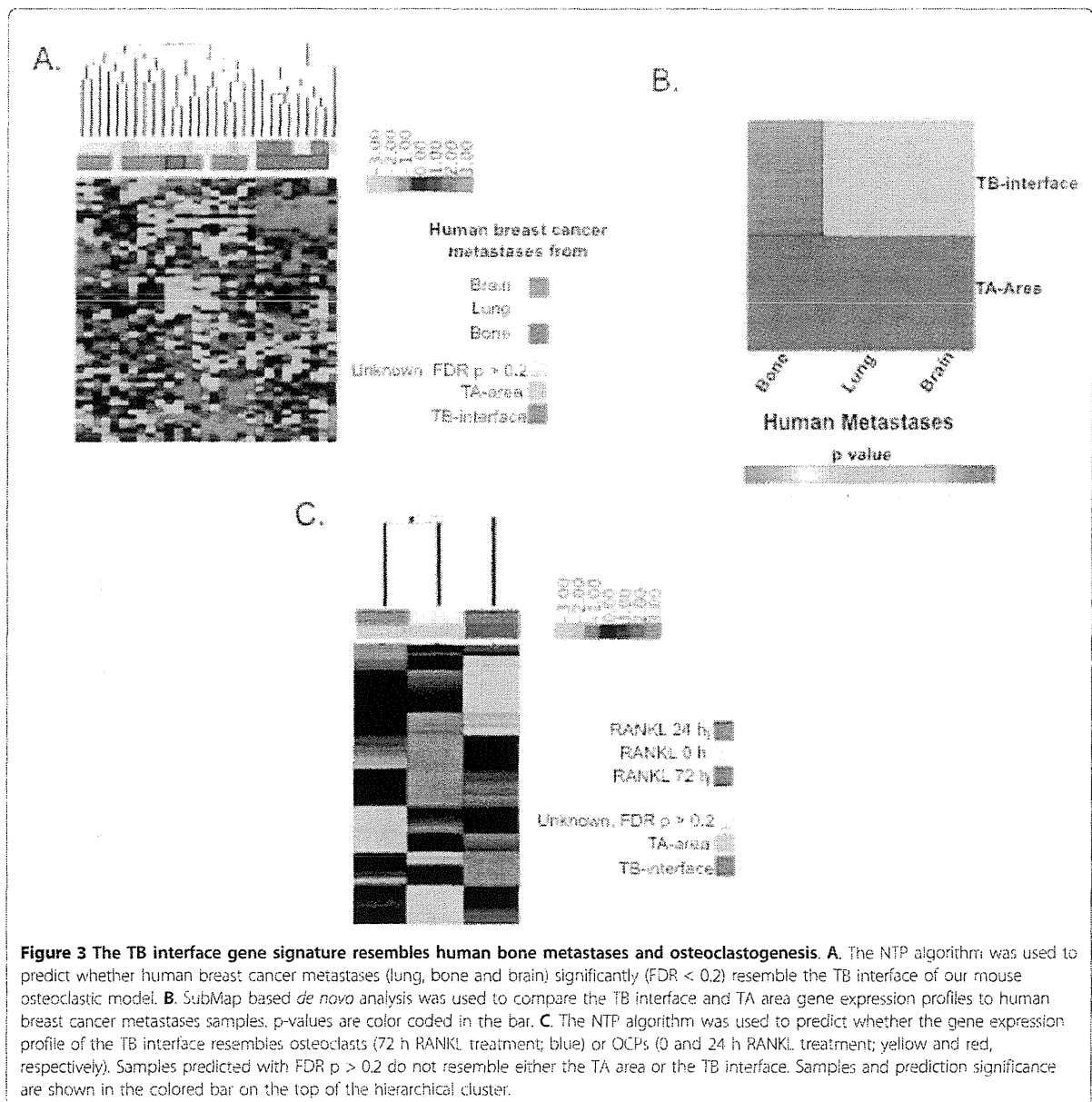


**Figure 3 The TB interface gene signature resembles human bone metastases and osteoclastogenesis.** **A.** The NTP algorithm was used to predict whether human breast cancer metastases (lung, bone and brain) significantly (FDR < 0.2) resemble the TB interface of our mouse osteoclastic model. **B.** SubMap based *de novo* analysis was used to compare the TB interface and TA area gene expression profiles to human breast cancer metastases samples. p-values are color coded in the bar. **C.** The NTP algorithm was used to predict whether the gene expression profile of the TB interface resembles osteoclasts (72 h RANKL treatment; blue) or OCPs (0 and 24 h RANKL treatment; yellow and red, respectively). Samples predicted with FDR p > 0.2 do not resemble either the TA area or the TB interface. Samples and prediction significance are shown in the colored bar on the top of the hierarchical cluster.

These data suggest that Bmp-10 mediated TGF- $\beta$  superfamily signaling is active at the TB interface but not in the TA area. Future studies specifically over-expressing and knocking-down members of the TGF- $\beta$  signaling pathway will be required to specifically determine the role of TGF- $\beta$  signaling at the TB interface.

Pathways identified using KEGG analysis that were significantly (FDR p < 0.05) associated with our osteolytic model are shown in Table 4. Interestingly, the Wnt-signaling pathway is significantly associated with the TB signature (Figure 4B), and it appears to be inhibited. Indeed, two Wnt pathway antagonists (Wif1 and Sfrp4) are

expressed greater than 2-fold at the TB interface for all the mouse cell lines (data not shown). Among the four most down-regulated genes at the TB interface, relative to the TA area, two are Wnt pathway agonists (Wnt8b and Wnt2). These data suggest that the Wnt signaling pathway is active in the TA area but inhibited in the TB interface. Again, future studies specifically over-expressing and knocking-down members of the Wnt signaling pathway may be performed to further elucidate the role of Wnt signaling at the TB interface and in the TA area.

We also performed enrichment analysis of the TB signature using MSigDB canonical pathway database and

**Table 3 GO terms significantly associated with TB signature.**

GO ID	Alias	BH	p-value	Statistic
GO:0007219	Notch signaling pathway	0.001	2.65e-05	78.7
GO:0007155	Cell adhesion	0.001	3.39e-06	56.3
GO:0022610	Biological adhesion	0.001	3.39e-06	56.3
GO:0007178	Transmembrane receptor protein serine/threonine kinase signaling pathway	0.001	3.63e-06	77.0
GO:0007249	I-kappaB kinase/NF-kappaB cascade	0.001	4.49e-05	93.6
GO:0005164	Tumor necrosis factor receptor binding	0.001	4.49e-05	93.6
GO:0002761	Regulation of myeloid leukocyte differentiation	0.005	0.00052	96.3
GO:0045637	Regulation of myeloid cell differentiation	0.005	0.00052	96.3
GO:0007179	Transforming growth factor beta receptor signaling pathway	0.008	0.0014	93.5
GO:0017015	Regulation of transforming growth factor beta receptor signaling pathway	0.008	0.0014	93.5

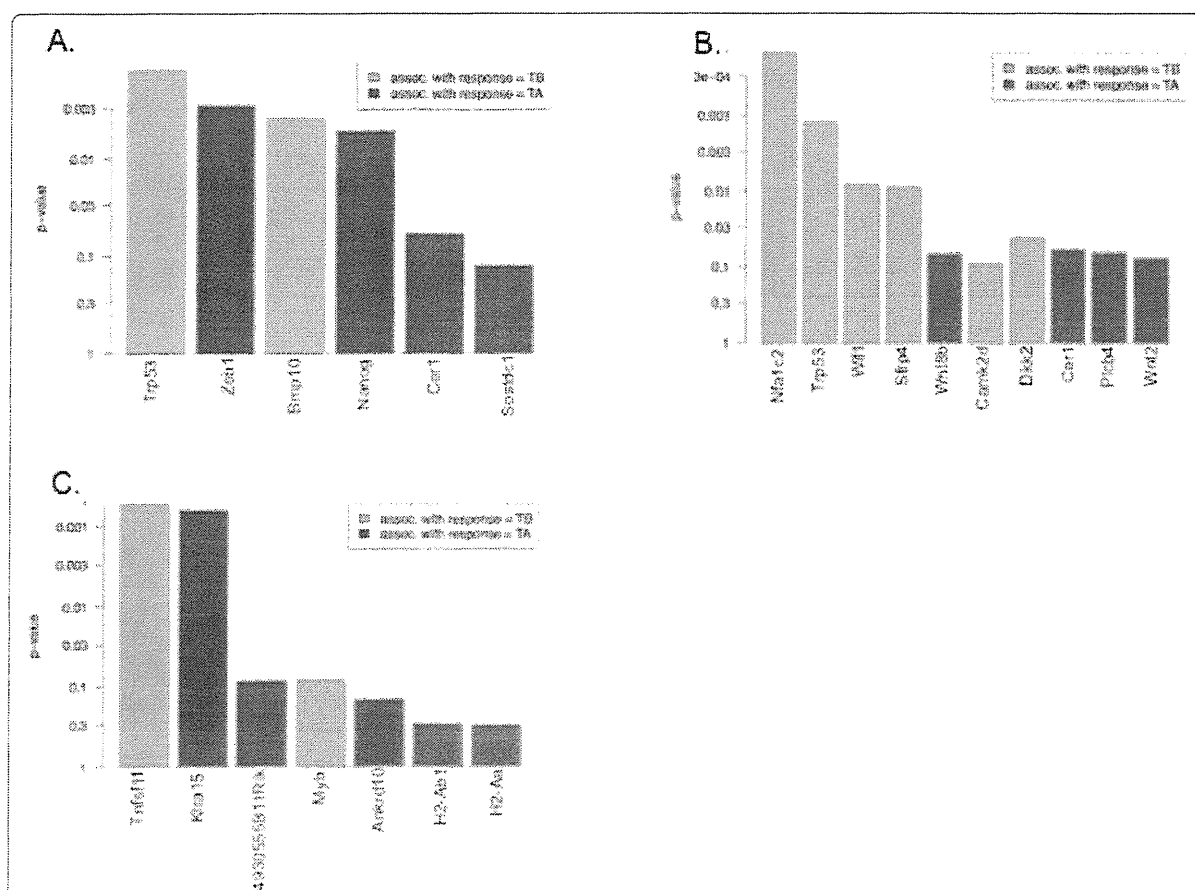


**Figure 4 Genes involved in pathways related to the TB interface and the TA area and prediction of a therapeutic agent that targets the TB interface.** p-values of pathway-specific genes enriched in the TB signature and in the TA area are plotted in green and red, respectively. Differential expression of genes in: **A.** the TGF-β pathway as determined using the GO database; **B.** the Wnt-signaling pathway using the KEGG pathway database; and **C.** the myeloid proliferation and self-renewal pathway [46] using MSigDB. All the enrichment analyses were done using GlobalTest package software. **D.** Connectivity Map analysis predicted cyclophosphamide as a candidate drug against the TB interface gene signature with 4 instances. All four instances fall in or near the red area (represented by black lines in the bar on the bottom), which suggests that cyclophosphamide reverses the TB interface gene expression signature.

**Table 4 KEGG pathways significantly associated with TB-signature**

KEGG ID	Alias	p-value	BH	Statistic
04060	Cytokine cytokine receptor interaction	7.60e-05	0.003	75.3
01100	Metabolic pathways	3.88e-05	0.003	52.8
05016	Huntington's disease	9.74e-05	0.003	57.9
04310	Wnt signaling pathway	1.07e-04	0.003	72.0
00061	Fatty acid biosynthesis	1.26e-04	0.003	98.2
04912	GnRH signaling pathway	1.26e-04	0.003	57.6
04020	Calcium signaling pathway	3.59e-04	0.007	67.1
05010	Alzheimer's disease	4.15e-04	0.007	66.5
04650	Natural killer cell mediated cytotoxicity	5.35e-04	0.008	60.9
04012	ErbB signaling pathway	6.28e-04	0.009	59.9

GlobalTest package [37,38]. Among the pathways significantly associated with the TB interface (Table 5) were myeloid proliferation and self-renewal [46]. Consistently, two genes (Rankl and Myb) highly expressed at the TB interface were significantly associated with this pathway (Figure 4C) [45]. This data further corroborates the NTP analysis comparing osteoclasts to our TB signature (Figure 3C) and provides additional evidence for a role of osteoclastogenesis at the TB interface.

#### Prediction and validation of therapeutic targets using the TB signature

To predict a therapeutic agent that specifically targets the TB interface, we queried Connectivity Map database [39] using the TB gene signature. Probeset identifiers from the Affymetrix Mouse Genome 430A 2.0 array were mapped to Affymetrix Human Genome U133A array. This was then used to query the Connectivity Map database. Of the 6,100 potential therapeutic candidates, cyclopenthiiazide had the most highly significant negative mean connectivity scores. In other words, cyclopenthiiazide was predicted to reverse the gene expression signature of the TB interface (Figure 4D). This analysis suggests that cyclopenthiiazide may be a

potential agent against human osteoclastic bone metastasis. Future studies aim to address this possibility by therapeutically dosing our mouse model with cyclopenthiiazide and monitoring for changes in the TB microenvironment.

#### Discussion

##### Mouse Model of the Osteolytic Microenvironment in Breast Cancer

Animal models that faithfully recapitulate aspects of human breast cancer-specific bone metastasis provide powerful tools to study the complex molecular mechanism(s) by which breast cancer cells metastasize to and interact with the bone microenvironment [47,48]. Previously, we developed mouse models of bone osteolysis for prostate and breast cancer by implanting syngeneic tumor cells onto the calvaria of animals using a simple surgical technique. These models produced osteolytic lesions at the TB interface of the implant region, thereby allowing us to explore the cellular and molecular interactions between malignant cells and skeletal tissue [11,12,15]. Because the tumor cells are implanted directly into the bone microenvironment (albeit, at an atypical location for breast cancer bone metastasis), it was important to confirm that the

**Table 5 MSigDB pathway signatures significantly associated with TB signature**

Alias	p-value	BH	Statistic
INTRINSICPATHWAY	0.0004	0.0007	96.9
BLOOD_CLOTTING_CASCADE	0.0004	0.0007	96.9
HSIAO_LIVER_SPECIES_GENES	0.0004	0.0007	96.9
TPA_SENS_MIDDLE_DN	0.0004	0.0007	96.9
TPA_SENS_LATE_DN	0.0004	0.0007	96.9
TPA_SENS_EARLY_DN	0.0004	0.0007	96.9
HSA04610_COMPLEMENT_AND_COAGULATION_CASCADES	0.0004	0.0007	96.9
BROWN_MYELOID_PROLIF_AND_SELF_RENEWAL	0.0062	0.010	60.2
BROWN GRAN MONO DIFFERENTIATION	0.0121	0.017	38.9
KAMMINGA_EZH2_TARGETS	0.0521	0.068	65.2

interactions observed in our model reflect those observed between metastatic human breast cells and the bone microenvironment. Building on our previous work, we now demonstrate that the TB microenvironment in our model appears very similar to that of human breast cancer bone metastases based on gene expression data. As such, this mouse model can be readily used to study the cellular and molecular mechanisms driving human breast cancer metastasis and osteolysis. Furthermore, this model also provides a powerful preclinical setting to test cyclophosphamide and other therapeutic agents that specifically target breast cancer osteolysis.

#### Gene Expression Profile Analysis

There has been tremendous growth in both the development of high-throughput microarray technology to measure gene expression in tissue and cells and in high-dimensional methods to analyze such data [49,50]. Together with this, many of the gene expression microarray data sets generated from different labs are now available in open-access databases [21,51], which enables the comparison and integration of data acquired from different batches, laboratories and experimental platforms [52]. Importantly, this has opened up opportunities to perform cross-species comparisons of mouse models and human disease [30].

In the current study, we applied microarray technology to generate a signature specific to the TB interface of our mouse model. The robustness of our TB-signature is supported by the fact that it was derived from a common set of genes regulated at the TB interface across a heterogeneous set of three mouse breast cancer cell lines. Combining gene expression profiling and molecular pathology, we demonstrated that the TB interface of our model truly represents the tumor microenvironment and not the normal bone microenvironment. Subsequent cross-species comparative transcriptomic analysis demonstrated that many human bone metastases samples are associated with the TB interface in a statistically significant manner. Importantly, there was no association between our breast TB interface and human brain or lung metastases. Together, these data demonstrate that our model specifically mimics human breast (and not lung or brain) cancer bone metastases. Furthermore, analysis of a panel of human breast cancer cell lines predicted 16 that have similar gene expression characteristics to those of the 4T1 tumors. This suggests that our osteolytic model may be adapted to study human breast cancer bone metastasis directly using any of these 16 human cell lines.

#### Pathways involved in the Breast Cancer Osteolytic Microenvironment

The TGF- $\beta$  pathway has a well established role in bone metastasis [53], and previously we demonstrated the

importance of TGF- $\beta$  signaling in the TB interface using our model [12]. Here, we demonstrate that the TGF- $\beta$  receptor 1 is expressed and that the TGF- $\beta$  pathway is active in tumor cells and osteoclasts at the TB interface. On the other hand, TGF- $\beta$  signaling is not active in the TA area [12]. Interestingly, the TGF- $\beta$  signaling ligand Bmp10 [54] is highly expressed at the TB interface and TGF- $\beta$  pathway inhibitors (i.e., *Sostdc1* [55] and *Cer1* [56]) are suppressed at the TB interface. These data suggest that Bmp-10 is responsible for mediating TGF- $\beta$  pathway activation at the TB interface.

The canonical and noncanonical Wnt signaling pathways are involved in the formation, growth and development of normal bone [57] and bone metastasis [58]. Activation of canonical Wnt signaling through  $\beta$ -catenin both promotes osteoblast differentiation and inhibits osteoclast formation and bone resorption [59]. Our KEGG pathway enrichment analysis showed a significant association of the Wnt signaling pathway at the TB interface. Indeed, we observed that Wnt pathway antagonists - *Wif1*, which is associated with decreased bone mineral density [60], and *Sfrp4*, which is associated with the suppression of osteoblast proliferation [61] - were over-expressed at the TB interface. Furthermore, we observed a down-regulation of the Wnt pathway ligands *Wnt2* [62] and *Wnt8b* [63] at the TB interface relative to the TA area. Together these data suggest that our mouse model exhibits (i) Wnt pathway activation in the TA area and (ii) increased bone resorption and suppressed bone formation (at least in part through Wnt pathway activation) at the TB interface.

Osteoclasts are derived from hematopoietic precursor cells of the myeloid lineage upon CSF-1 stimulation followed by RANKL-mediated maturation [43]. In our current study, we used a publicly available microarray dataset from RANKL-differentiated OCPs. Interestingly, we found that the gene expression profile of *in vitro* differentiated osteoclasts (72 h RANKL treatment) was similar to that of the TB interface. In addition, pathway analysis using the MSigDB showed an enrichment of the TB-signature in a myeloid cell line model [46] (Figure 4C). Overall, these results suggest that osteolysis is operative at the TB interface of our mouse model.

#### Prediction of a Therapeutic Agent that Targets the TB interface

The identification of new therapeutic agents that inhibit the establishment of tumor cells in the TB microenvironment will benefit patients with breast cancer bone metastases [5]. This will require a thorough understanding of the mechanisms governing breast-to-bone metastasis to determine appropriate biological targets for intervention. In one example, we previously demonstrated that TGF- $\beta$  signaling activity may provide such a target as pathway attenuation in our mouse model led to a reduction in